Journal of Controlled Release 361 (2023) 455–469

Contents lists available at ScienceDirect

Journal of Controlled Release

journal homepage: www.elsevier.com/locate/jconrel

Lipid nanoparticle-mediated messenger RNA delivery for ex vivo engineering of natural killer cells

Stefania Douka [a], Lisa E. Brandenburg [a], Cristina Casadidio [a,b], Johanna Walther [a], Bianca Bonetto Moreno Garcia [a,c], Jan Spanholtz [d], Monica Raimo [d], Wim E. Hennink [a], Enrico Mastrobattista [a,*], Massimiliano Caiazzo [a,e,*]

[a] Pharmaceutics division, Utrecht Institute for Pharmaceutical Sciences (UIPS), Faculty of Science, Utrecht University, Universiteitsweg 99, 3584, CG, Utrecht, the Netherlands
[b] School of Pharmacy, Drug Delivery Division, University of Camerino, CHiP Research Center, Via Madonna delle Carceri, 62032 Camerino, MC, Italy
[c] Department of Biophysics, Paulista School of Medicine, Federal University of São Paulo, São Paulo 04023-062, Brazil
[d] Glycostem Therapeutics B.V., Kloosterstraat 9, 5349 AB Oss, the Netherlands
[e] Department of Molecular Medicine and Medical Biotechnology, University of Naples "Federico II", Via Pansini 5, 80131 Naples, Italy

ARTICLE INFO

Keywords:
Natural killer cells
cancer immunotherapy
mRNA delivery
Lipid nanoparticles
Polyplexes
Electroporation

ABSTRACT

Natural killer (NK) cells participate in the immune system by eliminating cancer and virally infected cells through germline-encoded surface receptors. Their independence from prior activation as well as their significantly lower toxicity have placed them in the spotlight as an alternative to T cells for adoptive cell therapy (ACT). Engineering NK cells with mRNA has shown great potential in ACT by enhancing their tumor targeting and cytotoxicity. However, mRNA transfection of NK cells is challenging, as the most common delivery methods, such as electroporation, show limitations. Therefore, an alternative non-viral delivery system that enables high mRNA transfection efficiency with preservation of the cell viability would be beneficial for the development of NK cell therapies. In this study, we investigated both polymeric and lipid nanoparticle (LNP) formulations for eGFP-mRNA delivery to NK cells, based on a dimethylethanolamine and diethylethanolamine polymeric library and on different ionizable lipids, respectively. The mRNA nanoparticles based on cationic polymers showed limited internalization by NK cells and low transfection efficiency. On the other hand, mRNA-LNP formulations were optimized by tailoring the lipid composition and the microfluidic parameters, resulting in a high transfection efficiency (~100%) and high protein expression in NK cells. In conclusion, compared to polyplexes and electroporation, the optimized LNPs show a greater transfection efficiency and higher overall eGFP expression, when tested in NK (KHYG-1) and T (Jurkat) cell lines, and cord blood-derived NK cells. Thus, LNP-based mRNA delivery represents a promising strategy to further develop novel NK cell therapies.

1. Introduction

Recent developments in cancer immunotherapy have shown that our own immune system can be engineered to eliminate both hematological malignancies and solid tumors [1]. This can be achieved either by monoclonal antibodies targeting immune checkpoint inhibitors (ICIs) or adoptive cell therapy (ACT) [2]. Nevertheless, ACT is a more promising therapeutic solution in which allogeneic or autologous cells are expanded ex vivo to be infused into the patient intravenously (IV) [1]. In early development, tumor-infiltrating lymphocytes (TILs) as well as lymphokine-activated killer cells (LAK) were mainly applied in ACT [3]. Nowadays, the field has evolved to T-cell receptor (TCR) engineered cells and, most importantly, chimeric antigen receptor (CAR) engineered T cells (CAR-T), of which several products approved by the U.S. Food and Drug Administration (FDA) and European Medicines Agency (EMA) are on the market to target B-cell lymphoma, multiple myeloma, and other hematological malignancies [4,5].

However, CAR-T cell therapies face various limitations, such as toxicity, the clinical challenge, and a prohibitive price covering the production, administration, and logistics of autologous products [6,7]. Therefore, growing interest is focused on natural killer (NK) cells as an alternative to CAR-T cells for cancer immunotherapy, since early

* Corresponding authors.
E-mail addresses: e.mastrobattista@uu.nl (E. Mastrobattista), m.caiazzo@uu.nl (M. Caiazzo).

https://doi.org/10.1016/j.jconrel.2023.08.014
Received 28 February 2023; Received in revised form 28 June 2023; Accepted 8 August 2023
Available online 14 August 2023

preclinical and clinical data have demonstrated strong efficacy and an excellent safety profile [8,9]. Clinical-grade off-the-shelf NK cell therapies can be generated from multiple allogeneic sources, induce minimal damage to healthy tissues, with low risk of graft versus host disease (GvHD) and neurotoxicity [10,11]. Moreover, NK cells produce a different set of cytokines, not related to cytokine release syndrome (CRS) [12]. Notably, NK cell therapies can leverage the specificity of tumor antigen targeting in combination with innate anti-tumor function [9]. Off-the-shelf allogeneic NK cell products, could represent a cost-effective solution [10].

Unlike T cells, NK cells are a subtype of innate immune lymphoid cells which do not express antigen-specific receptors, and eliminate tumor cells directly, by generating lytic granules containing granzyme B and perforin, or by direct receptor-mediated apoptosis, or indirectly, through cytokine secretion [6,13,14]. Their cytotoxic action depends on the net balance of stimulatory and suppressive signals modulated by activating and inhibitory receptors, respectively [15]. Activating receptors such as NKp30, NKp44, NKp46, DNAM-1, NKG2C, and NKG2D recognize ligands on the surface of cancer cells and then "turn on" NK cells [16]. Conversely, inhibitory receptors, like NKG2A and the killer immunoglobin-like receptor family (KIR), recognize the major histocompatibility complex (MHC) class I molecules on the surface of healthy cells, therefore blocking NK cell activation [15,17]. Through their complex receptor system, NK cells are able to kill aberrant cells characterized by loss of surface MHC molecules and simultaneous upregulation of stress ligands, via the "missing-self" response [18,19]. Additionally, engagement of the CD16a (FCγRIIIA) receptor on the NK cell surface with opsonized immunoglobulin (Ig)G antibodies via the Fc region results in antibody-dependent cellular cytotoxicity (ADCC), leading to potent antitumor responses [20,21]. Thanks to their highly cytotoxic, non MHC-restricted, effector function, NK cells have great potential for ACT, representing a less cytotoxic alternative to allogenic T cells towards tumor cells [9,18].

NK therapies have shown clinical benefit, mostly for the treatment of hematological malignancies. However, effectively treating solid tumors remains a challenge [9]. In the immunosuppressive tumor microenvironment (TME), malignant cells secrete cytokines that impair NK cell migration and function [22]. Among other molecules, transforming growth factor-β (TGFβ) can downregulate degranulation, cytokine secretion and metabolism of NK cells [15]. To overcome these challenges, new strategies are being developed not only to improve NK cell resistance to immunosuppression but also to boost their tumor targeting and infiltrating cytotoxicity [23]. This is achievable by knocking-out inhibitory receptors like KIR and NKG2A or by (over)expressing activating receptors like CD16 and CXCR4 through NK cell engineering [24]. For this purpose, a highly efficient and safe technology to modify NK cells is urgently needed.

Messenger RNA (mRNA) represents a promising approach for therapeutic purposes [25,26]. Unfortunately, NK cells are hard-to-transfect cells, and the already established transfection methods show drawbacks [24,25]. For instance, electroporation is a well-established non-viral delivery method, that introduces DNA or RNA molecules into cells by temporarily increasing the cell membrane permeability. It has been already used in clinical development of NK cells by delivering NKG2D (clinicaltrials.gov ID: NCT03415100) and CD19 (NCT01974479) CAR mRNA in peripheral blood NK (PBNK) cells [27]. However, studies have shown that electroporation cause phenotypical alterations on NK cells that may influence therapeutic efficacy [28]. Thus, recent efforts to develop safer and more effective delivery technologies have shifted the focus towards synthetic nanoparticles for transfection [29,30].

In the present study, we explored the use of polymeric and lipid nanoparticles (LNPs) loaded with mRNA to transfect NK cells, evaluating their efficiency as well as their in vitro safety profile. The selection of the cationic polymers used in this study was based on previously reported data from our group. The triblock *co*-polymer pHDPA and the homopolymer pDMAEMA showed good transfection profile in dendritic and ovarian carcinoma cells, respectively [31,32]. Alternatives of these polymers were also studied, such as the diethylethanolamine-based pHDePA triblock co-polymer, its homopolymer pHPMA-DEAE, and a PEGylated form of pDMAEMA. After synthesis and characterization of the mentioned polymers, the resulting enhanced green fluorescent protein (eGFP) mRNA-polyplexes were applied to the easy-to-transfect human embryonic kidney 293 T (HEK293T) cells and subsequently to two NK cell lines (KHYG-1 and NK92). In parallel, starting from previously established mRNA-LNP formulations, we performed optimization tuning the lipid composition as well as the mRNA encapsulation method, to successfully deliver eGFP-mRNA to KHYG-1 cells [33]. Eventually, we identified a promising mRNA formulation based on lipoplexes for mRNA transfection of NK cells.

2. Materials and methods

2.1. General reagents

Unless stated otherwise, all chemicals and reagents were purchased from Sigma-Aldrich (Zwijndrecht, the Netherlands) and used without further purification. The solvents were obtained from Biosolve (Valkenswaard, the Netherlands) and dried by activated molecular sieves (4 Å). Carbonic acid 2-dimethylamino-ethyl ester 1-methyl-2-(2-methacryloylamino)-ethyl ester (HPMA-DMAE) [34], 2-diethylamino-ethyl ester 1-methyl-2-(2-methacryloylamino)-ethyl ester (HPMA-DEAE) [35], N-[2-(2-pyridyldithio)]ethyl methacrylamide (PDTEMA) [36], and 2-azidoethylmethyacryl-amide (AzEMAm) [37] were synthesized as previously reported. Linear polyethyleneimine (PEI, Mw 25 kDa) was obtained from Polysciences (Hirschberg an der Bergstraße, Germany). Ionizable lipids (bis(2-octyldodecyl) 3,3′- ((4-(4-methylpiperazin-1-yl) butyl)azanediyl)dipropionate) (C24) [38], and 8-[(2-hydroxyethyl)[6-oxo-6-(undecyloxy)hexyl]amino]-octanoic acid 1-octylnonyl ester (SM-102; Lipid 8) were purchased from DC Chemicals (Shanghai, China), and 1-octylnonyl 8-[(2-hydroxyethyl)[8-(nonyloxy)-8-oxooctyl] amino]octanoate (Lipid 5) was obtained from Cayman Chemical (Michigan, USA) [33]. Stigmasterol was obtained from Avanti Polar Lipids (Alabama, USA) and 1,2-distearoyl-sn-glycero-3-phosphocholine (DSPC) from Lipoid (Ludwigshafen, Germany). 1,2-Dimyristoyl-rac-glycero-3-methoxypolyethylene glycol-2000 (DMG-PEG2K) was purchased from NOF (Frankfurt, Germany). CleanCap® eGFP-mRNA (5moU) and Cy5-eGFP-mRNA were obtained from Trilink Bio-Technologies (San Diego, USA). Lipofectamine3000™, non-sterile Phosphate Buffered Saline (PBS), Slide-A-lyzer® Dialysis cassettes (Extra Strength) (MWCO: 10 kDa), Hoechst 33342, and Quant-iT™ RiboGreen™ RNA Assay Kit were purchased from Thermo Fisher Scientific (Bleiswijk, the Netherlands). RPMI 1640 medium with L-glutamine was obtained from Capricorn Scientific (RPMI-A, Ebsdorfergrund, Germany), α-MEM with (deoxy)ribonucleotides and UltraGlutamine from Lonza (Verviers, Belgium), and recombinant human interleukin-2 with "Improved Sequence" from Miltenyi Biotec (Bergisch Gladbach, Germany). Zombie NIR™ viability stain was purchased from BioLegend (Uithoorn, The Netherlands). ^{1}H NMR and spectra were recorded on an Agilent 400 Hz NMR spectrometer (Agilent Technologies, Santa Clara, CA, USA). Chemical shifts are reported as δ values and are given in ppm. Calibration was done using the residual solvent signals (^{1}H: δ 2.50 ppm for DMSO-d_6, ^{1}H: δ 7.26 ppm for $CDCl_3$ and ^{1}H: δ 4.79 ppm for D_2O). The spectra were analysed using MestReNova Software version 12.0.1–20,560.

2.2. Polyplexes

2.2.1. pHDPA

The triblock *co*-polymer p(HPMA-DMAE-*co*-PDTEMA-*co*-AzEMAm) (pHDPA) was synthesized by free radical polymerization (Fig. S1) as previously described [39]. The molecular weight and polydispersity index (PDI) were determined by gel permeation chromatography (GPC),

as described below. The copolymer composition was determined by ^{1}H NMR in D_2O (Fig. S2) by comparing the integrals at δ 4.37 ppm (bs, O$\underline{CH_2}CH_2$, 2H, HPMA-DMAE), δ 7.34–8.45 ppm (m, pyridyl proton group, 4H, PDTEMA), and δ 3.49 ppm (m, $\underline{CH_2CH_2}N_3$, 4H, AzEMAm).

2.2.2. pHDePA

The triblock *co*-polymer p(HPMA-DEAE-*co*-PDTEMA-*co*-AzEMAm) (pHDePA) was synthesized by free radical polymerization (Fig. S3), similar to the previously reported pHDPA [39]. The polymer was synthesized using a monomer-to-initiator (AIBN) molar ratio (M/I) of 20. The molar feed ratio of monomers was 77/22/11 as 220 mg (0.77 mmol) HPMA-DEAE, 56.7 mg (0.22 mmol) PDTEMA, 17 mg (0.11 mmol) AzEMAm were dissolved in dry DMSO (1 mL) with 3.6 mg (0.022 mmol) AIBN in an airtight Schlenk flask. After three vacuum-N_2 cycles, the polymerization occurred at 75 °C for 24 h under N_2 atmosphere. The resulting orange mixture was dropped in cold diethyl ether and the formed precipitate was redissolved in DMF (1–5 mL). This procedure was repeated 3 times. The polymer was then dissolved in 10 mM NH_4OAc (1–5 mL) buffer pH 5.0. After extensive dialysis (8 kDa MWCO) against 10 mM NH_4OAc buffer pH 5.0 (last step with 5 mM), at 4 °C, the polymer was collected after freeze-drying. The molecular weight and PDI were determined by GPC, as described in section 2.4.1. The copolymer composition was determined by ^{1}H NMR in DMSO-d_6 (Fig. S4) by comparing the integrals at δ 4.71 ppm (bs, O$\underline{CH_2}CH_2$, 2H, HPMA-DEAE), δ 7.2–8.48 ppm (m, pyridyl proton group, 4H, PDTEMA), and δ 3.69 ppm (m, $\underline{CH_2CH_2}N_3$, 4H, AzEMAm).

2.2.3. pHPMA-DEAE

Poly(carbonic acid 2-diethylamino-ethyl ester 1-methyl-2-(2-methacryloylamino)-ethyl ester) (pHPMA-DEAE) was synthesized similar as previously described [35], by free radical polymerization (Fig. S5) and at a M/I molar ratio of 400. Briefly, in an airtight Schlenk flask, 916 mg HPMA-DEAE (3.2 mmol) and 1.3 mg AIBN (0.008 mmol) were dissolved in dry DMSO (1 mL). After three vacuum-N_2 cycles, the polymerization occurred at 70 °C for 24 h under N_2 atmosphere. The resulting orange solution was mixed with 10 mM NH_4OAc (1 mL) buffer pH 5 and subsequently extensively dialyzed (3 kDa MWCO) against the same buffer for 3 days. Next, pHPMA-DEAE was freeze-dried and obtained as a fluffy white powder. ^{1}H NMR ($CDCl_3$): δ = 6.3 ppm (1H, OC$\underline{NH}CH_2$), 4.7 ppm (1H, NHCH$_2\underline{CH}$CH$_3$), 4.2 ppm (2H, OC=OO$\underline{CH_2}CH_2$N), 3.4–2.9 ppm (2H, OCNH$\underline{CH_2}$), 2.7 ppm (2H, OC=OOCH$_2\underline{CH_2}$N), 2.6 ppm (3H, NHCH$_2$CH$\underline{CH_3}$), 1.9 ppm (2H, CH$_3$C$\underline{CH_2}$CCH$_3$), 1.2 ppm (4H, 2 x N$\underline{CH_2}$CH$_3$), 1.0 ppm (6H, 2 x NCH$_2\underline{CH_3}$) (Fig. S6).

2.2.4. P_5D_{39}

The $(PEG)_2$-ABCPA polymer, composed of two arms of polyethylene glycol (PEG) chains of MW 5 kDa and 4,4′-azobis(4-cyanopentanoic acid) (ABCPA) as azoinitiator for free radical polymerization (Fig. S7), was synthesized as described previously [40]. Briefly, the $(PEG)_2$-ABCPA polymer (1 eq.) and DMAEMA (256 eq.) were dissolved in dry DMF (9 mL) in an airtight Schlenk flask, to result in a monomer concentration of 300 mg/mL. After three vacuum-N_2 cycles, the reaction mixture was placed in an oil bath at 70 °C and stirred for 24 h under N_2 atmosphere. The polymer solution was transferred into a dialysis bag (MWCO 14 kDa) and dialyzed against water for 2 days at 4 °C. The final PD polymer was collected after freeze-drying, and obtained as a white powder with a yield of 90%. The synthesized polymer was characterized by ^{1}H NMR spectroscopy (Fig. S8) and GPC.

2.2.5. pDMAEMA

The homopolymer poly(2-(dimethylamino)ethyl methacrylate (pDMAEMA) was synthesized as previously described and was characterized by ^{1}H NMR spectroscopy (Fig. S9) and GPC [41].

2.2.6. Polyplex formulation

Polymer stock solutions were prepared in 20 mM HEPES buffer pH 7.4 at 10 mg/mL for pHDPA, pHDePA, and pHPMA-DEAE and 5 mg/mL for PEI, PEG-pDMAEMA, and pDMAEMA. In a typical experiment, the mRNA polyplexes were prepared by mixing through manual pipetting the cationic polymer in 20 mM HEPES buffer pH 7.4 with the 5-methoxyuridine (5moU)-modified mRNA encoding for eGFP in 20 mM HEPES buffer pH 7.4 with 1:1 volume ratio, according to the respective N/P ratio. The resulting polyplexes were incubated on ice for 15 min before they were added to the cells. The polyplexes were characterized for particle size, PDI, and ζ-potential.

Regarding PEGylated and chemically crosslinked pHDPA, the following procedure was followed; the mRNA polyplexes were prepared at an N/P molar ratio of 4, with a final mRNA concentration of 100 μg/mL. PEG-BCN was synthesized as previously described [39] and was dissolved in 20 mM HEPES buffer pH 7.4 at 10 mg/mL. First, pHDPA (12 μL) was diluted with 88 μL HEPES buffer and this solution was subsequently added to 40 μg mRNA diluted with 60 μL 20 mM HEPES buffer pH 7.4, vortexed for 5 s, and incubated for 10 min on ice. Next, PEG-BCN (153.9 μL) was added to the polyplex dispersion and incubated at RT for 2 h. Finally, the polyplexes were crosslinked by the addition of half a molar to PDS groups DTT (10 μL; 5 mM in water) and incubated for 1 h at RT. After the addition of 40 μL sucrose (50% in water, 5% final concentration), the polyplexes were frozen using liquid nitrogen and subsequently freeze-dried. The resulting powder was resuspended in RNase-free water (400 μL) for a final mRNA concentration of 100 μg/mL before the polyplexes were added to the cells.

2.3. Lipid nanoparticles

LNPs were prepared using a NanoAssemblr® microfluidic mixer (Precision Nanosystems, Vancouver, Canada), as depicted in Fig. S10. Briefly, the different lipids were dissolved in EtOH at molar ratios of 50:10:38.5:1.5 (ionizable lipid:DSPC:steroid:DMG-PEG2K) (Fig. 2A) while the 5moU-modified mRNA encoding for eGFP (1 mg/mL stock solution) was diluted with 6.25 mM NaOAc pH 5 to a final concentration of 33 ng/μL. The two solutions were mixed at a volume ratio of 1:1.5 or 1:3 (EtOH:aqueous) and a total flow rate (TFR) ranging from 4 to 11 mL/min. After mixing, the resulting LNPs were dialyzed against phosphate-buffered saline (PBS, pH 7.4) in Slide-A-lyzer® Dialysis cassettes (Extra Strength) (10 kDa MWCO) for at least 12 h and stored at 4 °C until use. The formulations were characterized for particle size, PDI, ζ-potential and RNA encapsulation efficiency.

2.4. Characterization

2.4.1. Gel permeation chromatography (GPC)

To determine the molecular weight of the synthesized polymers, GPC was performed using two linked PLgel 5 μm mixed-D columns (Polymer Laboratories, UK) on an Alliance 2695 (Waters, the Netherlands) chromatography system, with column temperature set to 65 °C, coupled to a refractive index detector. DMF containing 10 mM LiCl was used as eluent at a rate of 1 mL/min. The sample concentration employed was 3 mg/mL, and PEG polymers of different molecular weight and with a narrow distribution (PSS, Germany) were used as calibration standards. Data analysis was performed by the Waters Empower 32 software.

2.4.2. Gel retardation assay

To examine the polyplex stability and mRNA release in different N/P ratios, polyplexes were prepared as described in section 2.2.6. and diluted with 20 mM HEPES buffer (pH 7.4) to a final mRNA concentration of 20 μg/mL. To examine the release potential in physiological conditions, the polyplexes were mixed with heparin sodium salt solution at a final concentration of 2.5 mg heparin/mL. Next, the samples were incubated at 37 °C for 45 min and subsequently mixed with 4 μL of 6× orange DNA loading dye and loaded into a 1% agarose gel in Tris-acetate-EDTA (TAE) buffer containing Midori Green (DNA/RNA stain; NIPPON Genetics Europe). After electrophoresis at 120 V for 30 min, the

gel was analysed by a ChemiDoc™ Imager (Bio-Rad Laboratories Inc., Hercules, CA) using Image Lab software (version 6.0.1).

2.4.3. Dynamic light scattering (DLS) and ζ-potential

The size and the PDI of the polyplexes and the LNPs were measured with DLS using a Zetasizer Nano-S at a 90° angle (Malvern ALV CGS-3, Worcestershire, UK) at 25 °C and the Zetasizer software 7.13. The ζ-potential was determined using a Zetasizer Nano-Z (Malvern ALV CGS-3, Worcestershire, UK) with universal ZEN 1002 'dip' cells at 25 °C. Polyplexes were measured in 20 mM HEPES buffer (pH 7.4) at an mRNA concentration of 15 μg/mL, while LNPs were measured in PBS (pH 7.4).

2.4.4. mRNA encapsulation efficiency

The mRNA encapsulation by LNPs was determined using the Quant-iT™ RiboGreen™ RNA Assay Kit according to manufacturer protocol; briefly, mRNA-LNP formulations were diluted 100 times and subsequently incubated at RT with Quant-iT™ assay reagent, in the presence or absence of 0.5% Triton X-100 to measure the total and the unencapsulated mRNA, respectively. The standards and the samples were measured using a Jasco FP-8300 spectrophotometer (excitation wavelength: 485 nm /emission wavelength: 530 nm). Based on the calibration curves of the standards with and without triton, the encapsulation efficiency was calculated by the following formula: *EE% = ((total mRNA-unencapsulated mRNA)/total mRNA) x 100%.*

2.5. Cell culture

HEK293T, NK-92, and Jurkat cells were obtained from the American Type Culture Collection (ATCC, Manassas, Virginia, USA). KHYG-1 cells were acquired from DSMZ (ACC725, Braunschweig, Germany). HEK293T cells were cultured in Dulbecco's Modified Eagle Medium (DMEM) supplemented with 10% (*v/v*) of fetal bovine serum (FBS). KHYG-1 cells were cultured in Roswell Park Memorial Institute (RPMI) 1640 medium with glutamine, 10% FBS (*v/v*), and 160 U/mL recombinant human interleukin 2 (IL-2), at a density of 0.5×10^6 cells/mL. NK-92 cells were cultured in α-Minimum Essential Medium (alpha-MEM) with glutamine and ribonucleosides, supplemented with 12.5% (*v/v*) horse serum, 12.5% (*v/v*) FBS and 1000 U/mL IL-2, at a density of 0.5×10^6 cells/mL. Jurkat cells were cultured in RPMI 1640 medium supplemented with 10% (*v/v*) heat-inactivated FBS. Cord blood-derived NK cells were obtained from Glycostem Therapeutics and cultured as previously reported [42,43]. All cells were cultured at 37 °C in a humidified atmosphere containing 5% CO_2.

2.6. mRNA transfection assay

The transfection experiments were performed over three consecutive days as follows. First, 2.5×10^4 cells/well were seeded in a flat bottom 96-well plate and were incubated overnight at 37 °C with 5% CO_2. On the day of transfection, polyplexes or LNPs were added without refreshing the cell medium, and the cells were incubated for 24 h at 37 °C with 5% CO_2. The amount of mRNA was 250 ng/well for polyplexes and 500 ng (low dose) and 1 μg (high dose) per well for LNPs. For the LNPs, the dose was calculated according to the obtained volume of the formulation after dialysis and the amount of mRNA, assuming 100% encapsulation efficiency. On day three, the preparation for analysis with flow cytometry or/and confocal fluorescence microscopy was performed. As a positive control, Lipofectamine3000™ was used according to the manufacture's protocol with mRNA concentration at 150 ng/well for polyplexes and 500 ng/well for LNPs.

2.7. Electroporation

Electroporation was performed using a BTX ECM 830 square electroporator (Holliston, US). Briefly, 2×10^6 cells were harvested and washed with 1 mL of 0.01% DMSO in Opti-MEM. Next, the cell pellet was resuspended in 200 μL 0.1% DMSO in Opti-MEM and subsequently added to a 4 mm BTX aluminum cuvette (Holliston, US) equipped with 20 μg mRNA/mL (4 μg mRNA/cuvette). Next, the cells were electroporated using one pulse of 1450 V for 50 μs and were then transferred into a 6-well plate containing 2 mL of complete medium per well and incubated for 24 h at 37 °C with 5% CO_2.

2.8. Flow cytometry (FC)

To assess the transfection efficiency, cell viability, and geometric mean fluorescence intensity (gMFI) of positive signals, cells were analysed using FC. First, cells were transferred into a U-bottom 96-well plate and washed with PBS (pH 7.4). To quantify the cytotoxicity, the cells were treated with Zombie NIR™ Fixable Viability dye (BioLegend), diluted 1:1000 according to the manufacturer's protocol, and were incubated at RT in the dark for 30 min. After incubation, the cells were washed with 0.5% bovine serum albumin (BSA) in PBS and subsequently fixed with 1% paraformaldehyde (PFA) in PBS for 10 min in RT. The fixed cells were kept at 4 °C until analysis with a BD FACSCanto™ II Flow Cytometry System (Franklin Lakes, USA), acquiring 10^4 events per well. The background signal from untreated cells was subtracted from the reported transfection efficiency of treated cells. The viability percentage was normalized based on the viability of the untreated cells (100%). The gating strategy is illustrated in Fig. S11.

2.9. Confocal live cell imaging

To visualize the eGFP expression or Cy-5 eGFP-mRNA uptake, cells were imaged with the confocal fluorescent microscope Yokogawa Cell Voyager CV7000s (Tokyo, Japan). After overnight incubation with the transfection mixture, cells were washed with PBS (pH 7.4) and incubated in the dark with 1:500 diluted Hoechst 33342 in Opti-MEM at 37 °C for 10 min to stain cell nuclei. Fluorescent images were analysed with ImageJ software.

2.10. Statistical analysis

Statistical analysis was performed using GraphPad Prism 9.5.0. The values are expressed as the mean ± standard deviation (SD). Means were compared using one-way ANOVA, unless indicated otherwise. Differences were considered statistically significant at $p < 0.05$.

3. Results and discussion

3.1. Polyplex-mediated mRNA transfection of NK cells

3.1.1. Polyplex formulation and characterization

To investigate the mRNA transfection potential of polyplexes in NK cells, first the cationic polymers pHDPA, pHDePA, pHPMA-DEAE, pDMAEMA, and PEG-pDMAEMA were synthesized as previously reported [35,39–41]. The synthesized polymers were characterized by ^{1}H NMR, and their molecular weight as well as their polydispersity (PDI) were evaluated by GPC (Table S1). The copolymer composition of the triblock *co*-polymers pHDPA and pHDePA was measured by the integration of the relative protons on ^{1}H NMR. The AzEMAm content was 28% and 26% for pHDPA and pHDePA, respectively, which is substantially higher than the feed composition of 11%. This is in accordance with the previous results of Lou et al. [39]. The yield of the polymerization of pHDPA and pHDePA was around 25%, possibly due to polymer loss during workup in combination with an incomplete monomer conversion. The latter can explain the higher final AzEMAm content since its smaller size makes it more reactive during free radical polymerization.

The polyplexes were prepared through self-assembly of the cationic polymers with mRNA via electrostatic interactions between the amine groups of the polymers and the phosphate groups of the mRNA. To study the influence of PEGylation and crosslinking, first the azide groups of

Table 1
Characteristics of mRNA polyplexes.

Polyplexes	N/P ratio	Size[a] (nm ± SD)	PDI[a]	ζ-potential[b] (mV ± SD)
pHDPA w PEG, crosslinked	4	199 ± 13	0.15	−21.0 ± 1.1
pHDPA w/o PEG, crosslinked	10	56 ± 0	0.25	−10.7 ± 0.8
pHDePA w/o PEG, crosslinked	10	164 ± 3	0.21	+14.3 ± 0.3
pHPMA-DEAE	10	185 ± 3	0.30	+20.1 ± 0.2
P_5D_{39}	10	77 ± 1	0.22	+13.0 ± 1.1
pDMAEMA	10	144 ± 1	0.27	+6.5 ± 0.4
PEI	40	138 ± 1	0.23	+17.5 ± 1.7

[a] Determined by DLS.
[b] Determined by Zetasizer.

pHDPA polyplexes were post-modified with PEG-BCN via copper-free click chemistry, followed by the addition of DTT to chemically crosslink the pyridine disulfide groups of the polymer. These polyplexes were then freeze-dried with sucrose as cryoprotectant and redispersed in nuclease-free water before their addition to the cells.

A significant parameter of mRNA polyplexes is the N/P ratio, i.e., the ratio of the amine groups of the polymer to the phosphate groups of the nucleic acid. Several studies have shown that the N/P ratio plays a critical role not only in the characteristics of the polyplexes but also in the transfection efficiency and viability of the transfected cells [44,45]. To examine the mRNA complexation and particle stability, different N/P ratios of pHDPA, pHDePA, pHPMA-DEAE, pDMAEMA, and P_5D_{39} polyplexes were analysed with an agarose gel electrophoresis. As shown in Fig. S12, mRNA complexation was achieved for all tested N/P ratios. After the addition of negatively charged heparin, the polyplexes formulated at all the examined N/P ratios released mRNA, demonstrating a reversible complexation. Although polyplexes prepared at higher N/P ratios show enhanced cellular uptake and endosomal escape, the excess of cationic polymer usually has a negative effect on cell viability [46,47]. To avoid potential toxicity, high N/P ratios were therefore excluded for the following transfection experiments. Thus, an N/P ratio of 10 was used to formulate pHDPA, pHDePA, pHPMA-DEAE, pDMAEMA, and P_5D_{39} polyplexes. PEGylated and crosslinked pHDPA polyplexes were formulated with an N/P ratio of 4, as previously described by Lou et al. [39]. For PEI polyplexes, an N/P ratio of 40 was selected, according to the transfection data published by Huh et al. [48].

As shown in Table 1, apart from pHDPA (with and without PEGylation and crosslinking) which resulted in the formation of polyplexes with a negative ζ-potential, the other polyplexes were positively charged and their size ranged from 138 to 199 nm (Table 1). Only, pHDPA without PEGylation and P_5D_{39} resulted in smaller particles of 56 nm and 77 nm, respectively.

3.1.2. mRNA-polyplex mediated transfection of HEK293T, KHYG-1 and NK-92 cells

To investigate the transfection efficiency of the mRNA polyplexes on NK cells, an easier-to-transfect cell line, the HEK293T cells, was used first. Lipofectamine3000™ and free mRNA in culture medium were tested as controls. As shown in Fig. 1A, pHDPA based polyplexes with or without post-modification were not able to transfect the HEK293T cells. Both polyplexes based on the PEGylated and the homopolymer of DMAEMA (P_5D_{39} and pDMAEMA) showed a transfection efficiency of 3% and 1%, respectively, while the HPMA-DEAE-based polyplexes (pHDePA and pHPMA-DEAE) resulted in around 0.5% eGFP-positive cells. Lipofectamine and PEI resulted in >50% eGFP-expressing cells. Regarding toxicity, all polymers preserved the viability of HEK293T cells at >95% except for P_5D_{39}, which showed cytotoxicity with a drop in viability to around 50% (Fig. 1B).

Next, polyplex-mediated mRNA delivery was assessed on NK cells (Fig. 1C). For this, only PEI, P_5D_{39}, and pHPMA-DEAE were screened on two NK cell lines, namely KHYG-1 and NK-92. Lipofectamine3000™ was used as control. Only a small number of NK cells were eGFP-positive (0% with PEI, ~0.5% with P_5D_{39}, and pHPMA-DEAE). Lipofectamine lipoplexes also showed minimal transfection efficiency (~0.05%) of NK cells, which is in accordance with previous work [28]. Similar to HEK293T cells, P_5D_{39} polyplexes were the only ones causing toxicity, as cell viability dropped to 66% and 85% for KHYG-1 and NK-92, respectively (Fig. 1D).

3.1.3. Evaluation of polyplex uptake by KHYG-1 cells

The low efficiency of mRNA transfection with polyplexes suggests limited particle uptake or limitations in the endosomal escape of the polyplexes and the release of the mRNA into the cytosol. To assess the uptake of these nanoparticles by NK cells, PEI, P_5D_{39}, and pHPMA-DEAE polyplexes containing Cy5-labeled mRNA encoding for eGFP were formulated, and the same transfection assay was performed on KHYG-1 cells. The results were then visualized by fluorescent microscopy 24 h after transfection (Fig. 1E). Cy5 was visualized by the red channel and shows particle tracking within KHYG-1 cells, and eGFP was visualized by the green channel indicating protein expression. As shown in Fig. 1E, a higher cellular uptake (Cy5 signal) of lipofectamine lipoplexes and P_5D_{39} polyplexes was observed. However, the lack of eGFP expression indicates that after 24 h incubation these polyplexes were still inside the endosome or mRNA has not been released yet [49]. Both PEI and pHPMA-DEAE polyplexes showed limited to absent cellular uptake, which explains the low transfection activity in NK cells.

3.2. Lipid nanoparticle-mediated mRNA transfection of NK cells

3.2.1. Screening of different ionizable lipids

Since the tested polymeric eGFP-mRNA nanoparticles showed limited expression of the reported gene into NK cells, we also tested the transfection potential of LNPs based on previously described formulations [33,50]. LNPs formulated with the ionizable lipids C24, Lipid 5, and SM-102 (Fig. 2A 1–3) at an N/P ratio of 3, were first tested on KHYG-1 cells to evaluate their influence on transfection efficiency and cell viability. A volume ratio of 1:1.5 (EtOH:aqueous) and a TFR of 4 mL/min were used during microfluidic formulation. As shown in Fig. 2B, LNPs with C24 achieved only 3% of eGFP-positive cells, when a high dose was used. LNPs composed of Lipid 5 and SM-102 ionizable lipids successfully transfected KHYG-1 cells, with the transfection efficiency ranging from 48% for Lipid 5 to 70% for SM-102 (Fig. 2B). Interestingly, SM-102 also resulted in higher gMFI, especially with high dose (Fig. 2D). However, since only one N/P ratio was used in this experiment, we further performed optimization steps to establish the optimal formulation parameters.

3.2.2. Optimization of the mRNA-LNPs

During optimization, the particles were characterized for size, PDI, and ζ-potential and the transfection efficiency, the intensity of eGFP expression (gMFI), and cell viability were evaluated by flow cytometry, as presented in Table 2 and Fig. S13. To identify the optimal ionizable lipid for transfection of KHYG-1 cells, LNPs of different N/P ratios for both Lipid 5 and SM-102 were screened. For SM-102, the LNPs of N/P 3 and 5 showed similar transfection efficiency, ranging from 82% to 84% depending on the dose. Differently, the N/P ratio played a critical role for Lipid 5, as N/P 5 significantly increased not only the transfection efficiency when compared to N/P 3, from 36% to 90% (low dose), but also the gMFI from 3 to 2819 a.u. (Table 2 and Fig. S13). The overall toxicity was not an issue, as cell viability was >95% when N/P of 3 and 5 were used for both ionizable lipids. It should also be mentioned that differences in N/P ratio did not influence the size of the particles, as the size for both SM-102 and Lipid 5 in N/P 3 and 5 ranged from 105 to 110 nm (Table 2). As expected, the ζ-potential slightly increased when a higher N/P ratio was used, from −3.5 to −2.7 mV and from −6.2 to

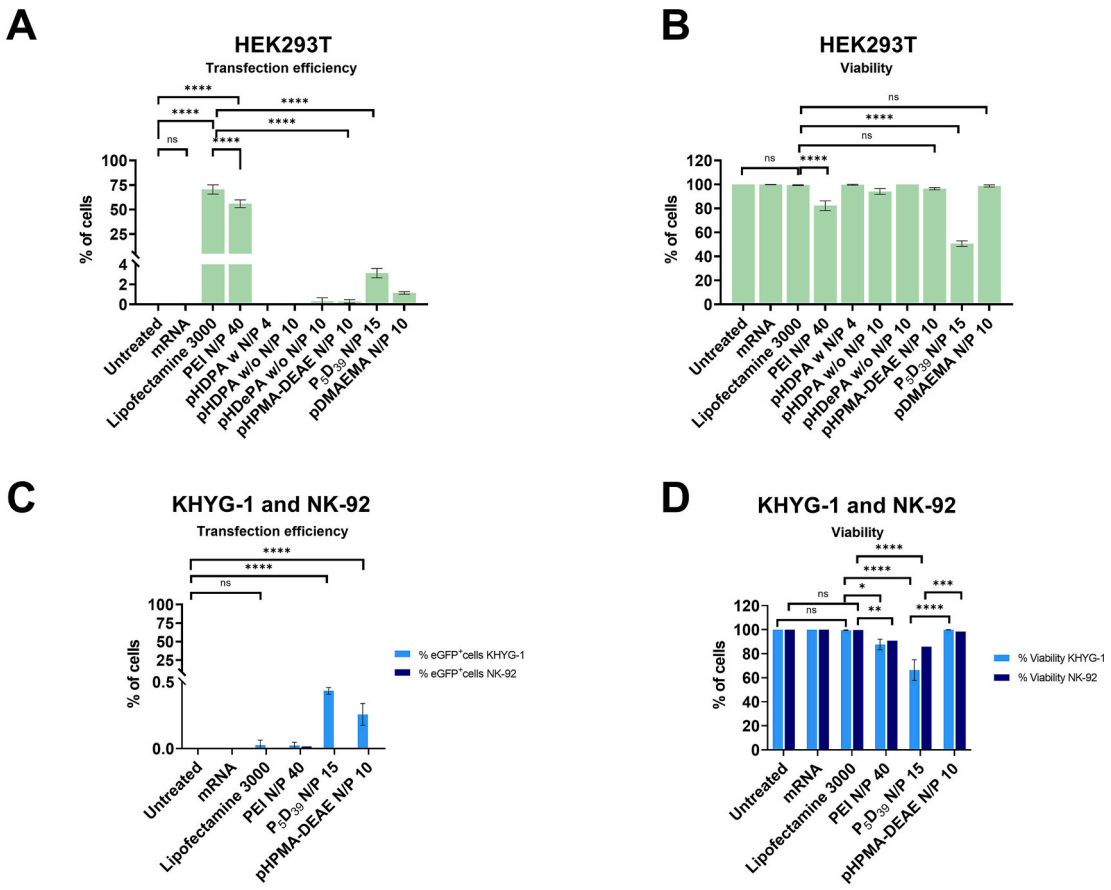

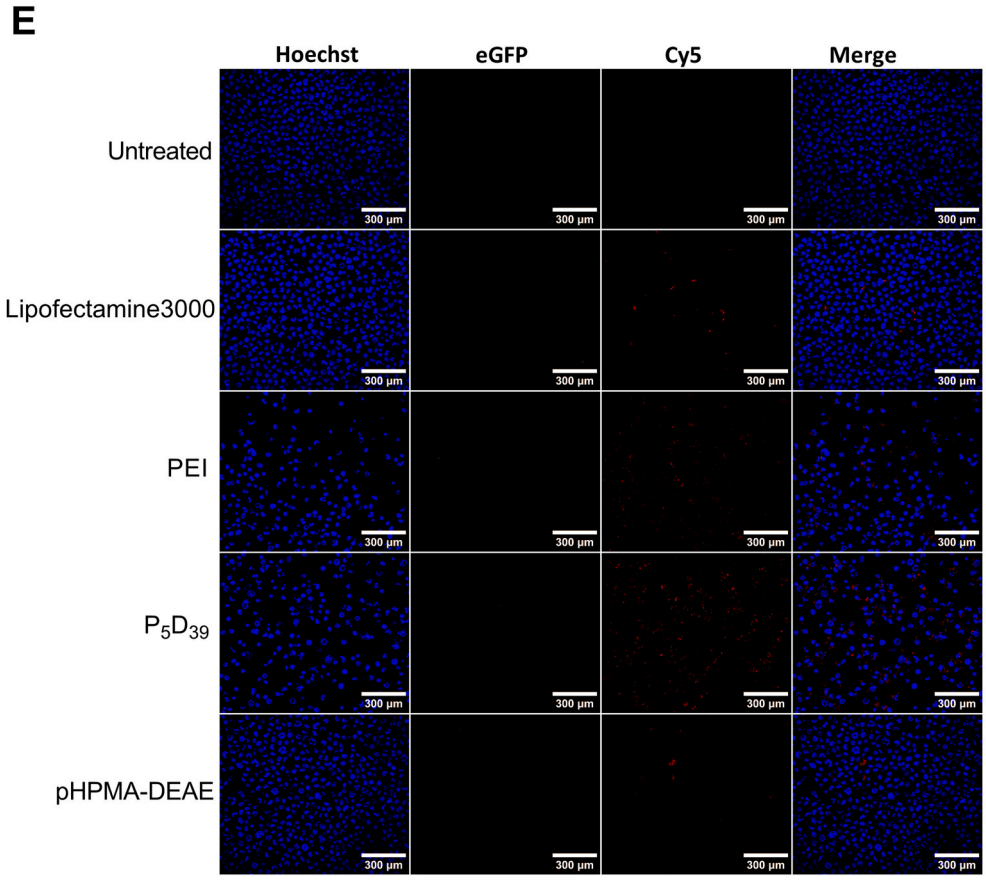

(caption on next page)

Fig. 1. Evaluation of transfection efficiency and cell viability by flow cytometry 24 h after transfection with different eGFP-mRNA polyplexes of HEK293T cells and two NK cell lines, KHYG-1 and NK-92. A) Evaluation of transfection efficiency by flow cytometry 24 h after treatment of HEK293T cells with eGFP-mRNA-polyplexes. B) Evaluation of viability of HEK293T cells 24 h after treatment with eGFP-mRNA-polyplexes, measured by flow cytometry. C) Evaluation of transfection efficiency by flow cytometry 24 h after treatment of NK cells with eGFP-mRNA-polyplexes. Light and dark blue bars represent the percentage of eGFP+ KHYG-1 and NK92 cells, respectively. D) Evaluation of viability of NK cells 24 h after treatment with eGFP-mRNA-polyplexes, measured by flow cytometry. Light and dark blue bars represent the percentage of KHYG-1 and NK92 viable cells, respectively. E) Fluorescence microscopy images of the PEI, P_5D_{39} and pHPMA-DEAE polyplexes, and Lipofectamine3000™ uptake by KHYG-1 cells. Cy5 labeled eGFP-mRNA was used to formulate the particles and uptake was studied 24 h after transfection. Cy5 (red channel) represents particle uptake and eGFP (green channel) represents protein expression. Scale bar represents 300 μm. $n = 3$ technical replicates, * = $p < 0.1$, ** = $p < 0.01$, *** = $p < 0.001$, and **** = $p < 0.0001$. (For interpretation of the references to colour in this figure legend, the reader is referred to the web version of this article.)

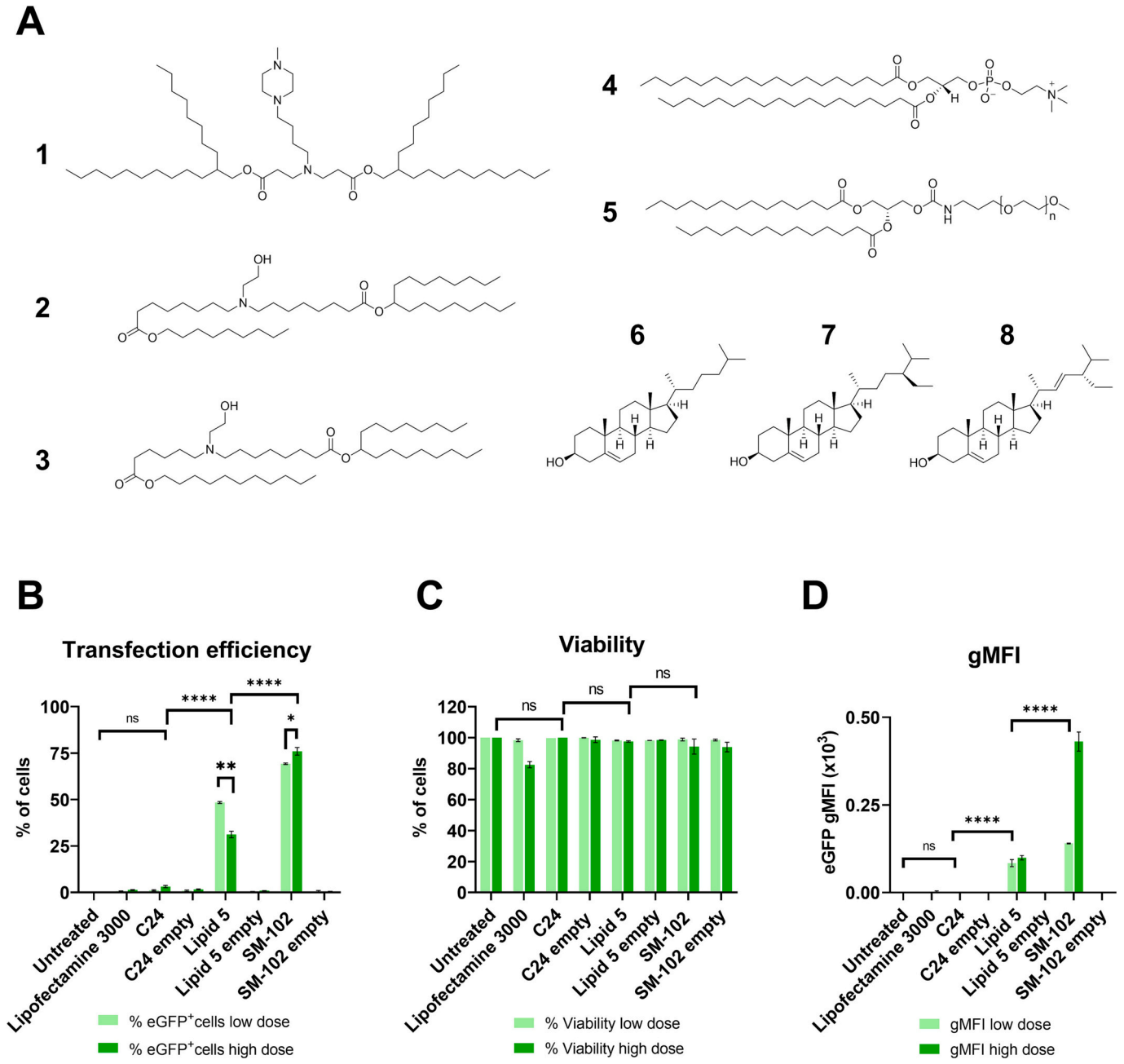

Fig. 2. mRNA delivery to KHYG-1 cells using LNPs formulations and screening different ionizable lipids. A) Lipids used during the LNP optimization: (1) C24, (2) Lipid 5, (3) SM-102, (4) DSPC, (5) DMG-PEG2k, (6) Cholesterol, (7) β-Sitosterol, and (8) Stigmasterol. B) Evaluation of transfection efficiency by flow cytometry 24 h after treatment of KHYG-1 cells with mRNA-LNPs formulated with the ionizable lipids C24, Lipid 5 and SM-102. The loaded particles are compared with empty LNPs. Light and dark green bars represent the percentage of eGFP-positive cells after treatment with low and high dose, respectively. $n = 3$ technical replicates, **** = $p < 0.0001$. Student's *t*-test was used for the statistical analysis of the transfection efficiency of Lipid 5 and SM-102 based LNPs with low vs high dose, * = $p < 0.05$, ** = $p < 0.01$. C) Viability of KHYG-1 cells 24 h after treatment with mRNA-LNPs formulated with the ionizable lipids C24, Lipid 5 and SM-102, measured by flow cytometry. Light and dark green bars represent the percentage of KHYG-1 viable cells after treatment with low and high dose, respectively. n = 3 technical replicates. D) gMFI of eGFP expression of KHYG-1 24 h after treatment with loaded and empty LNPs using the different ionizable lipids. n = 3 technical replicates, **** = p < 0.0001. Lipofectamine3000™ is used as control.

Table 2
Optimization of lipid nanoparticles.

Ionizable Lipid	N/P ratio	Steroid	TFR[a] (mL/min)	Volume ratio	Size[b] (nm ± SD)	PDI[2]	ζ-potential[c] (mV ± SD)	EE[d]	TE[e]		gMFI[f]		Viability	
									Low	High	Low	High	Low	High
SM-102	3	Cholesterol	4	1:1.5	105 ± 3	0.10	−3.5 ± 0.9	NT[g]	81%	86%	277	942	100%	99%
SM-102	5	Cholesterol	4	1:1.5	109 ± 3	0.22	−2.7 ± 0.3	NT	83%	84%	454	697	99%	98%
Lipid 5	3	Cholesterol	4	1:1.5	104 ± 2	0.24	−6.2 ± 1.4	NT	36%	46%	3	30	98%	99%
Lipid 5	5	Cholesterol	4	1:1.5	110 ± 5	0.25	−4.9 ± 1.9	76%	90%	87%	2819	2596	97%	95%
Lipid 5	5	Cholesterol	11	1:1.5	92 ± 17	0.49	−2.3 ± 1.4	85%	56%	70%	135	267	98%	99%
Lipid 5	5	β-Sitosterol	11	1:1.5	86 ± 13	0.48	−2.6 ± 0.6	53%	87%	84%	5143	4845	97%	94%
Lipid 5	5	Stigmasterol	11	1:1.5	82 ± 5	0.63	−6.1 ± 1.1	60%	36%	36%	26	21	98%	97%
Lipid 5	5	β-Sitosterol	9	1:1.5	137 ± 6	0.33	−2.8 ± 0.2	31%	30%	15%	3	0	95%	91%
Lipid 5	5	Cholesterol	9	1:3	89 ± 1	0.13	−2.8 ± 0.4	NT	77%	80%	1676	942	94%	98%
Lipid 5[h]	5	β-Sitosterol	9	1:3	151 ± 4	0.22	−7.1 ± 0.4	NT	92%	94%	19,745	13,553	99%	100%

[a] Total Flow Rate.
[b] Determined by DLS.
[c] Determined by Zetasizer.
[d] Encapsulation Efficiency.
[e] Transfection Efficiency.
[f] Mean Fluorescence Intensity of eGFP.
[g] NT = not tested.
[h] Final optimized LNP formulation.

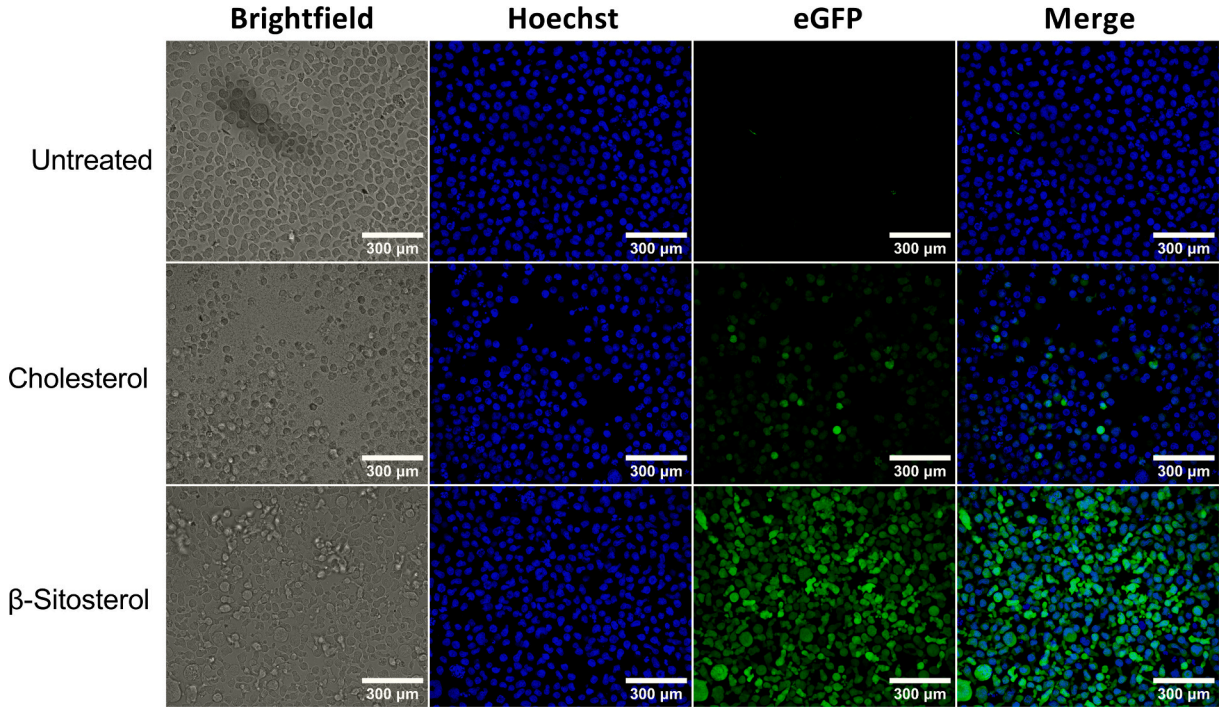

Fig. 3. Fluorescence microscopy images of KHYG-1 cells 24 h after transfection with a low dose (500 ng mRNA per well) of Lipid 5 N/P 5 based mRNA-LNPs formulated with either cholesterol or β-sitosterol. Scale bar represents 300 µm.

−4.9 mV for SM-102 and Lipid 5, respectively. Since the LNP formulation based on Lipid 5 showed higher expression intensity compared to SM-102 (gMFI 2819 over 454 a.u.), further optimization was pursued using Lipid 5 as the ionizable lipid at an N/P ratio 5.

Replacing cholesterol with its plant-based structural analogues β-sitosterol and stigmasterol (Fig. 2A 6–8) was previously reported to enhance endosomal escape and therefore protein expression [51,52]. In our hands, addition of stigmasterol to the formulation resulted in highly polydisperse particles with a PDI of 0.63, probably due to aggregation, that resulted in lower transfection efficiency (around 36%) and very low gMFI (Table 2 and Fig. S13). Incorporation of β-Sitosterol on the other hand, not only considerably improved transfection activity compared to cholesterol-based LNPs (87% versus 56% for low dose and 84% versus 70% for high dose), but it also significantly increased the total eGFP expression (Table 2 and Fig. S13). Specifically, the gMFI measured by FC showed a 38-fold increase for low dose that is in accordance with the fluorescent images in Fig. 3. As shown in Table 2, no significant differences could be observed in terms of size and ζ-potential for cholesterol and β-sitosterol based formulations, as they both resulted in 92 and 86 nm particles, respectively with a slightly negative ζ-potential of around −2 mV. Additionally, the mRNA encapsulation was higher when cholesterol was used as a steroid, therefore, the observed difference in eGFP expression can be explained by the morphology of the LNPs. Eygeris et al. have previously investigated the differences in morphology of cholesterol and phytosterol LNPs, using cryo transmission electron microscopy (Cryo-TEM), differential scanning calorimetry (DSC) and a

Table 3
Characteristics of the optimized mRNA-LNPs (Lipid 5/DSPC/β-sitosterol/DMG-PEG2K).

	Size[a] (nm ± SD)	PDI[a]	ζ-potential[b] (mV ± SD)	EE[c]
mRNA-LNPs	125 ± 1.4	0.18	−3.8 ± 1.1	84%

[a] Determined by DLS.
[b] Determined by Zetasizer.
[c] Encapsulation efficiency.

membrane fluidity assay, showing that β-sitosterol LNPs have a higher degree of lamellarity [53]. Accordingly, as shown by Patel et al., LNPs composed of phytosterols are polymorphic and multilamellar, showing different surface morphology, therefore, different lipid composition in the outer lipid layer compared with the with cholesterol ones. Their cryo transmission electron microscopy (Cryo-TEM) images clearly indicate that LNPs formulated with both cholesterol and natural analogues show a core-shell structure, with an amorphous core and a lamellar surface. However, LNPs with natural analogues, like β-sitosterol, exhibit a multifaceted surface compared to cholesterol-based LNPs that show an evenly curved outer layer. [51]. The structural change of the β- LNPs can increase the fragility of the particle and thus its fusion with the endosomal membrane, eventually enhancing mRNA cytosolic delivery [51,53].

Modifying the formulation parameters during microfluidic assembly of the LNPs also played an important role in optimization. Due to limitations in the settings of the microfluidic equipment, the TFR had to be reduced from 11 to 9 mL/min in order to compare the 1:1.5 with a higher volume ratio. When the TFR was lowered from 11 to 9 mL/min at a fixed volume ratio of 1:1.5 (EtOH:aqueous), a drop from 87% to 30% with low dose and from 84% to 15% with high dose was observed in transfected cells (Table 2 and Fig. S13). As shown in Table 2, the ζ-potential of the particles remained around −2 mV, however the size increased from 86 to 137 nm. This difference in particle size is expected since higher TFRs result in smaller particles [54,55]. Conversely, when the TFR was lowered to 9 mL/min while increasing the volume ratio from 1:1.5 to 1:3, the percentage of eGFP-positive cells was recorded at 92% and 94% (for low and high dose, respectively) (Table 2), which is the highest transfection efficiency observed in this study. By increasing the volume ratio, the amount of aqueous buffer increases as well. This results in higher solution polarity and therefore stronger self-assembly of the LNPs. This can potentially lead to smaller particle size, enhanced mRNA complexation and overall higher transfection efficiency. Finally, the 1:3 volume ratio led to higher gMFI levels and eGFP expression (Table 2 and Fig. S13).

Compared to the tested eGFP-mRNA-polyplexes of section 3.1.2, LNPs exhibited comparable results, with particle sizes ranging from 90 to 150 nm. Regarding polydispersity, LNPs formulated with both cholesterol and β-sitosterol demonstrated a narrow distribution, with polydispersity values ranging from 0.13 to 0.22. Polymeric nanoparticles showed similar levels of polydispersity. Nonetheless, a notable distinction between the two nanoparticle types was observed in terms of surface charge. Polyplexes displayed a highly negative charge, while LNPs exhibited a slightly negative charge closer to zero. This difference in ζ-potential emphasizes the significance of the particle charge, as it can influence the interaction with the NK cell membrane, potentially affecting crucial factors such as cellular uptake. The comparison of the characteristics of the two nanoparticle types can be found in Table S2.

The optimization revealed that the optimal lipids for the LNP formulation were the Lipid 5, DSPC, DMG-PEG2K and β-sitosterol. In addition, mRNA complexation with a N/P ratio of 5 and TFR of 9 mL/min with a volume ratio of 1:3 (EtOH-aqueous) were the optimal parameters during LNP microfluidics formulation. Besides the influence of lipid composition and formulation parameters, this optimization

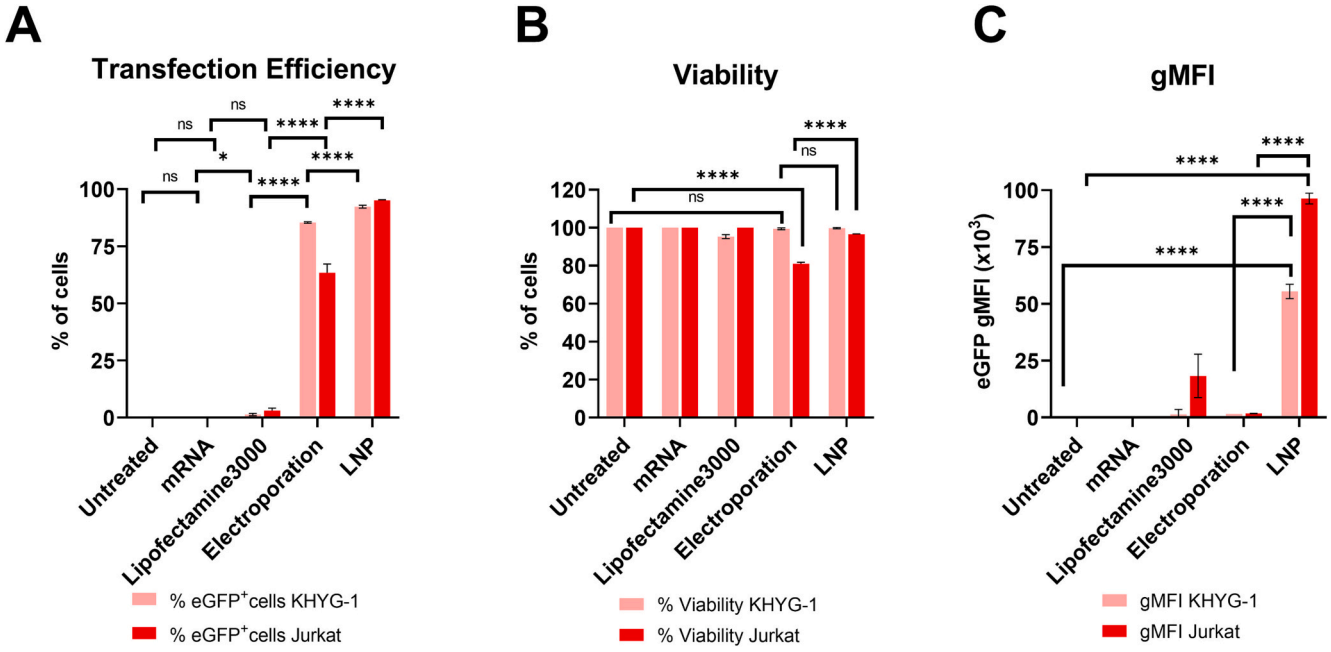

Fig. 4. Comparison of the optimized mRNA-LNPs with electroporation of free mRNA in KHYG-1 and Jurkat cells. A) Evaluation of transfection efficiency by flow cytometry of KHYG-1 and Jurkat cells 24 h after transfection with the optimized mRNA-LNPs (Lipid 5/DSPC/β-sitosterol/DMG-PEG2K, N/*P* = 5, TFR = 9 mL/min, and 1:3 EtOH:aqueous volume ratio), electroporation and Lipofectamine3000™. Pink and red bars represent the percentage of KHYG-1 and Jurkat eGFP-positive cells, respectively. B) Evaluation of KHYG-1 and Jurkat cells viability by flow cytometry 24 h after transfection with the optimized mRNA-LNPs (Lipid 5/DSPC/β-sitosterol/DMG-PEG2K, N/P = 5, TFR = 9 mL/min, and 1:3 EtOH:aqueous volume ratio), electroporation and Lipofectamine3000™. Pink and red bars represent the percentage of KHYG-1 and Jurkat viable cells, respectively. C) gMFI of eGFP expression 24 h after treatment with the optimized mRNA-LNPs (Lipid 5/DSPC/β-sitosterol/DMG-PEG2K, N/P = 5, TFR = 9 mL/min, and 1:3 EtOH:aqueous volume ratio), electroporation and Lipofectamine3000™. Pink and red bars represent the gMFI of KHYG-1 and Jurkat cells, respectively. $n = 3$ technical replicates, * = $p < 0.05$ and **** = $p < 0.0001$. (For interpretation of the references to colour in this figure legend, the reader is referred to the web version of this article.)

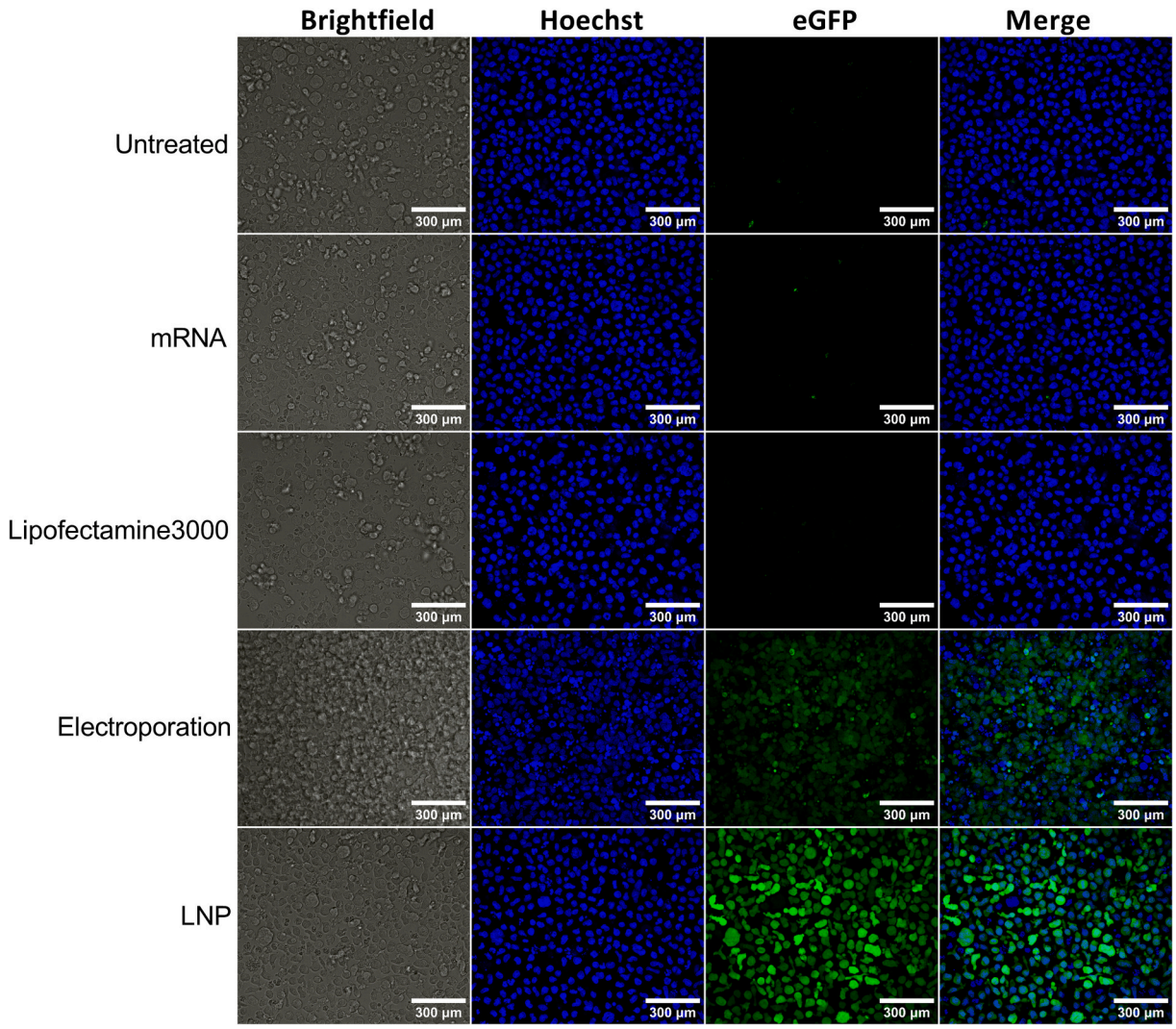

Fig. 5. Fluorescence microscopy images of KHYG-1 cells 24 h after transfection with Lipofetcamine3000™ lipoplexes, electroporation of free mRNA and low dose of the optimized mRNA-LNPs (Lipid 5/DSPC/β-sitosterol/DMG-PEG2K, N/*P* = 5, TFR = 9 mL/min, and 1:3 EtOH:aqueous volume ratio). Scale bar represents 300 μm.

showed that NK cell transfection is efficient with both tested mRNA doses. Therefore, the next experiments were performed using the lower dose (500 ng mRNA per well) of the optimized formulation.

3.2.3. Optimized LNPs show superior transfection parameters in KHYG-1 and Jurkat cells

The mRNA delivery efficiency of the LNPs, formulated using the optimized parameters (Lipid 5, N/P 5, β-sitosterol, TFR 9 mL/min, and 1:3 volume ratio), was compared to electroporation in two immune cell lines: KHYG-1 NK cells and Jurkat T cells. After full characterization of a new mRNA-LNPs batch (Table 3), KHYG-1 and Jurkat cells were incubated with this mRNA formulation following the transfection protocol, as described in section 2.6.

As shown in Fig. 4A and B, LNPs and electroporation resulted in 92% and 85% eGFP-positive KHYG-1 cells, respectively, while the cell viability was retained (>99%). Importantly, Fig. 4C and 5 shows that transfection with LNPs caused a 35-fold increase in gMFI over electroporation. As expected, free mRNA and lipofectamine lipoplex were unable to transfect KHYG-1 cells.

A similar pattern was observed in Jurkat cells. Fig. 4A shows that LNPs were superior to electroporation transfecting 95% of the cells compared to 63% of eGFP-positive electroporated cells. As expected, lipofectamine lipoplexes transfected only a low number of cells (~3%). In Fig. 4B, a drop in viability in electroporated cells was noticeable, as 20% of the cells died during treatment. Jurkat's viability dropped only by 4% when incubated with the LNPs. In contrast to KHYG-1 cells, the difference in gMFI measured by FC was even more pronounced as LNPs showed a 54-fold increase in eGFP expression compared to electroporation, as shown in Fig. 4C. A clear indication that mRNA-LNPs provide a strong intracellular eGFP expression is also shown in fluorescence images on Fig. 6.

These differences in transfection efficiency and gMFI can potentially be explained by the fact that cells are exposed to mRNA-LNPs for 24 h compared to the brief electroporation stimulus (50 μs with one pulse). Moreover, the low gMFI of electroporated KHYG-1 and Jurkat cells (Fig. 4B) can be a result of the harsh conditions of this treatment, which can permanently damage the cells and potentially the eGFP-mRNA. According to Wilk et al., electroporation has explicit off-target effects on NK cell phenotype, and Napotnik et al. have previously reported that electroporation, among others, can cause metabolic stress, and membrane and genomic damage [28,56]. These findings can also explain the differences in cell morphology of both electroporated KHYG-1 and Jurkat cells in Figs. 5 and 6. Finally, electroporation is known to cause partial precipitation of macromolecules like DNA and RNA after their interaction with metal cations from the cuvettes [57]. This can contribute to the reduction of mRNA availability and, thus, decreased protein expression. This indicates that LNPs show better cytocompatibility, superior transection efficiency and higher eGFP expression when

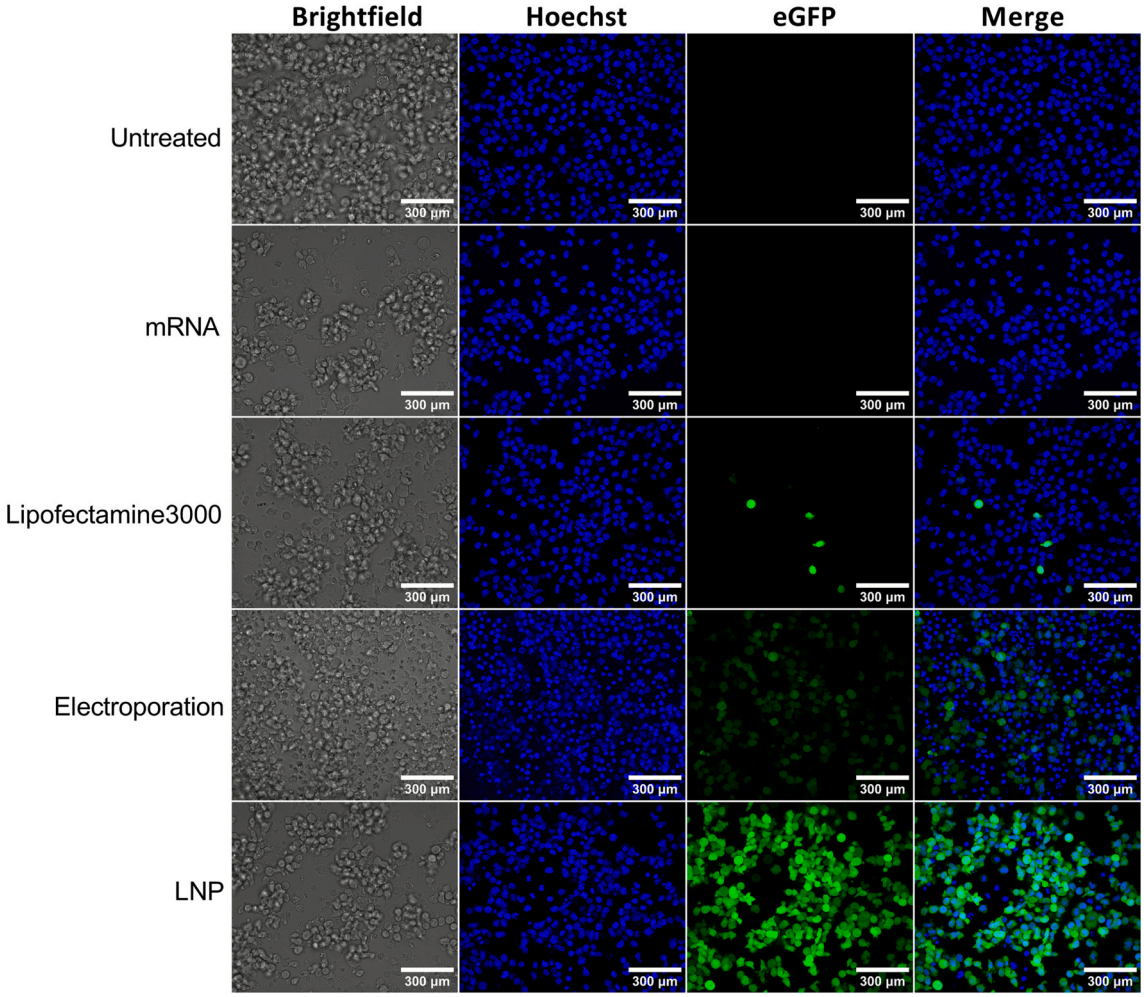

Fig. 6. Fluorescence microscopy images of Jurkat cells 24 h after transfection with Lipofetcamine3000™ lipoplexes, electroporation of free mRNA and low dose the optimized mRNA-LNPs (Lipid 5/DSPC/β-sitosterol/DMG-PEG2K, N/*P* = 5, TFR = 9 mL/min, and 1:3 EtOH:aqueous volume ratio). Scale bar represents 300 μm.

compared with electroporation and represents a promising tool for clinical development of engineered NK cells.

3.2.4. *Optimized LNPs efficiently transfect cord blood-derived NK cells*

In order to understand the potential translational value of our optimized eGFP-mRNA LNP formulation its efficacy was investigated in cord blood-derived NK cells. As depicted in Fig. 7, LNPs were superior to electroporation in terms of transfection efficiency, reaching 75% compared to 57% for electroporation (Fig. 7A). As for toxicity, both delivery technologies exhibited comparable high cell viability of 99.5% (Fig. 7B). However, a notable difference was observed in the intensity of eGFP expression, as shown in Fig. 7C, where the optimized LNPs resulted in a 5-fold increase in gMFI in comparison to electroporation.

Furthermore, fluorescence microscopy images were acquired to assess eGFP expression in the transfected NK cells. The images in Fig. 7D clearly depict the superiority of LNPs in inducing a higher level of protein expression, exhibiting a brighter signal compared to electroporation. These findings suggest that the optimized LNPs are more efficient in facilitating eGFP-mRNA delivery and subsequent protein expression in ex vivo-derived NK cells.

3.2.5. *Dose titration of the optimized mRNA-LNPs on the KHYG-1 NK cell line*

Meanwhile this paper was under revision, Nakamura et al. published that a Fluc-mRNA-LNP formulation successfully transfected another NK cell line, NK-92MI, in low doses ranging from 0.066 to 0.6 μg/mL. In addition, their findings suggest that NK-92MI viability is dose dependent [58]. Given the high dose of 500 ng mRNA-LNPs per well that was used for both optimization and evaluation of the transfection efficiency on KHYG-1, Jurkat and primary NK cells, a dose titration was performed to assess the mRNA delivery potential of the optimized LNPs (Lipid 5/DSPC/β-sitosterol/DMG-PEG2K, N/*P* = 5, TFR = 9 mL/min, and 1:3 EtOH:aqueous volume ratio) in lower mRNA doses. For this purpose, eGFP-mRNA-LNPs were formulated and tested in the KHYG-1 cell line at varying mRNA doses ranging from 1.9 to 500 ng per well (2.5×10^4 cells).

As shown in Fig. 8, the results reveal consistent high eGFP-mRNA transfection efficiency across all doses, with values ranging from 89% to 92%. Furthermore, cell viability remained constant at approximately 99% regardless of the mRNA dose. However, a notable trend was observed in the gMFI, indicating a reduction as the dose decreased, implying a diminishing level of cellular fluorescence. Specifically, the highest gMFI value of 55×10^3 was reported with the higher dose of 500 ng and the lowest value of 1.5×10^3 with the lower dose of 1.9 ng. Importantly, mRNA doses ranging from 15.6 to 250 ng per well, reached similar gMFI ranging from 15×10^3 to 30×10^3.

These findings suggest that while transfection efficiency and cell viability are maintained at high levels across the tested dose range, the mRNA dose is correlated with intracellular protein expression. In addition, doses lower than 500 ng showed great potential in both transfection efficiency and gMFI. To prevent the high production costs a standard dose lower than 500 ng mRNA per well will be considered in

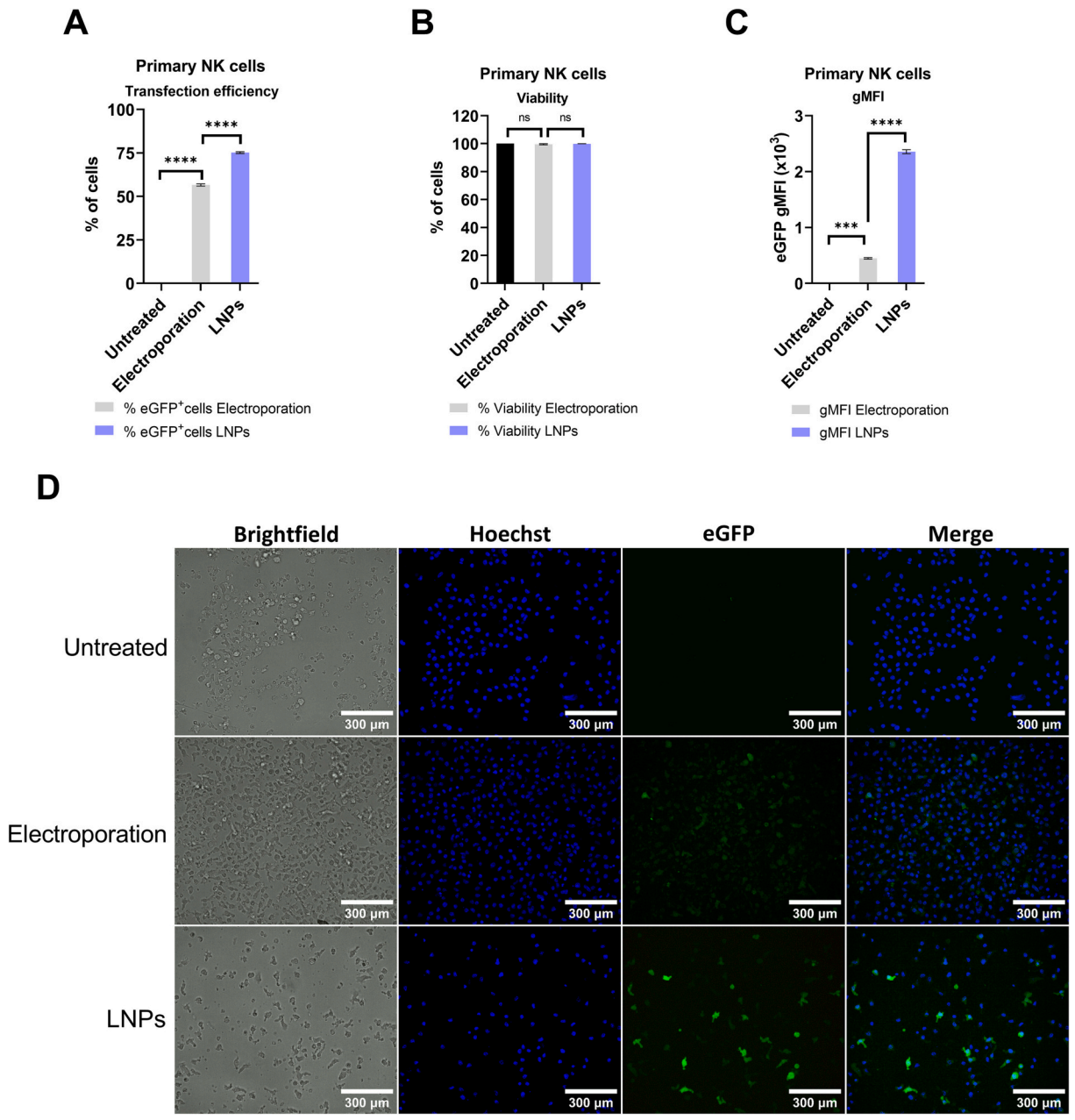

Fig. 7. Comparison of the optimized mRNA-LNPs with electroporation of free mRNA in cord blood-derived NK cells. A) Evaluation of transfection efficiency by flow cytometry of cord blood-derived NK cells 24 h after transfection with the optimized mRNA-LNPs (Lipid 5/DSPC/β-sitosterol/DMG-PEG2K, N/*P* = 5, TFR = 9 mL/min, and 1:3 EtOH:aqueous volume ratio), and electroporation. Grey and purple bars represent the percentage of NK eGFP-positive cells after mRNA delivery with electroporation and the optimized LNPs, respectively. B) Evaluation of cord blood-derived NK cells viability by flow cytometry 24 h after transfection with the optimized mRNA-LNPs (Lipid 5/DSPC/β-sitosterol/DMG-PEG2K, N/P = 5, TFR = 9 mL/min, and 1:3 EtOH:aqueous volume ratio), and electroporation. Grey and purple bars represent the percentage of NK cell viability after mRNA delivery with electroporation and the optimized LNPs, respectively. C) gMFI of eGFP expression 24 h after treatment of cord blood-derived NK cells with the optimized mRNA-LNPs (Lipid 5/DSPC/β-sitosterol/DMG-PEG2K, N/P = 5, TFR = 9 mL/min, and 1:3 EtOH:aqueous volume ratio), and electroporation. Grey and purple bars represent the gMFI after mRNA delivery with electroporation and the optimized LNPs, respectively. $n = 2$ technical replicates, *** = $p < 0.001$ and **** = $p < 0.0001$. D) Fluorescence microscopy images of cord blood-derived NK cells 24 h after transfection with electroporation of free mRNA and 500 ng per well of the optimized mRNA-LNPs (Lipid 5/DSPC/β-sitosterol/DMG-PEG2K, N/P = 5, TFR = 9 mL/min, and 1:3 EtOH:aqueous volume ratio). Scale bar represents 300 µm. (For interpretation of the references to colour in this figure legend, the reader is referred to the web version of this article.)

our future studies.

4. Conclusions

Currently, the main technology to deliver mRNA to NK cells in ongoing clinical trials is electroporation. However, drawbacks such as impact on the morphology and phenotype of electroporated cells, as well as on mRNA integrity, have shifted the focus to synthetic nanoparticles as transfection agents. In this study, we aimed to identify an mRNA delivery technology for ex vivo engineering of NK cells. Therefore, we compared polyplexes, LNPs, and electroporation for optimal eGFP-mRNA delivery. We demonstrated that mRNA polyplexes resulted in limited transfection efficiency and cellular uptake by NK cells. Conversely, LNPs showed promising results with cord blood-derived NK,

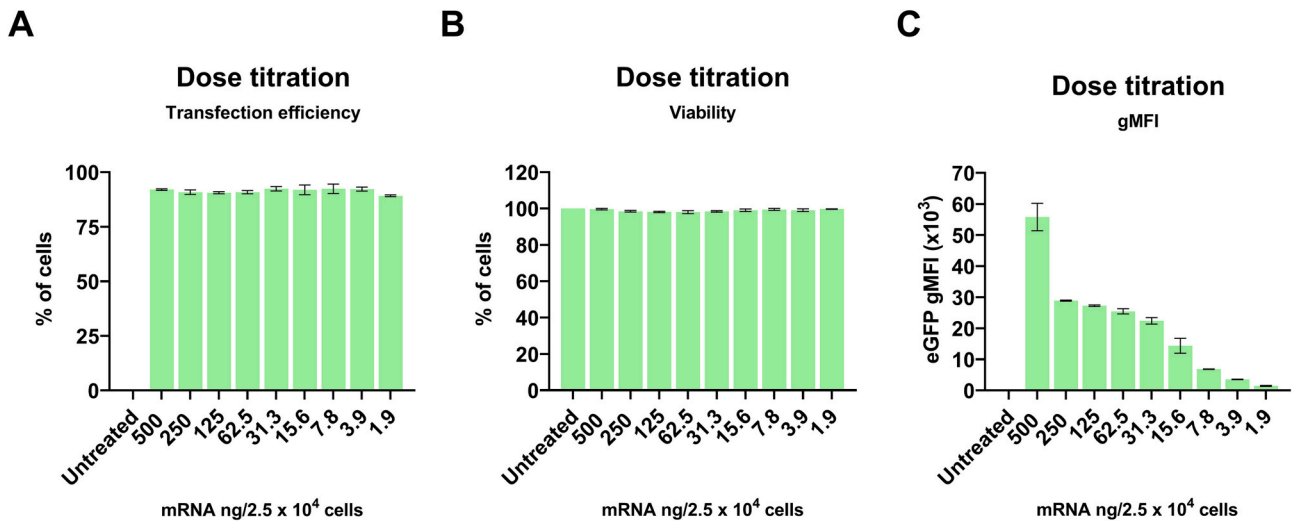

Fig. 8. Dose titration of eGFP-mRNA-LNPs (Lipid 5/DSPC/β-sitosterol/DMG-PEG2K, N/P = 5, TFR = 9 mL/min, and 1:3 EtOH:aqueous volume ratio) on KHYG-1 cells. A) Evaluation of transfection efficiency by flow cytometry 24 h after treatment of KHYG-1 cells with mRNA-LNPs in different doses. B) Viability of KHYG-1 cells 24 h after treatment with mRNA-LNPs in different doses, measured by flow cytometry. C) gMFI of eGFP expression of KHYG-1 24 h after treatment with mRNA-LNPs in different doses.

KHYG-1 and Jurkat cells. Specifically, when Lipid 5 was used as ionizable lipid. LNP optimization revealed that N/P 5, cholesterol replacement with β-sitosterol, a TFR of 9 mL/min, and a 1:3 (EtOH:aqueous) volume ratio increased not only the number of eGFP-positive cells but also the overall intracellular eGFP expression, within a broad range of mRNA doses. When compared with electroporation, improvements were observed in transfection efficiency, protein expression, and cell morphology. Further investigation is needed to assess the functionality of NK cells' receptors after treatment with the mRNA-LNPs, but this study shows the potential of LNPs for clinical development of novel NK cell therapeutics.

Funding

This work was supported by the Health Holland Organization [grant number LSHM19131].

CRediT authorship contribution statement

Stefania Douka: Conceptualization, Formal analysis, Methodology, Project administration, Validation, Visualization, Writing – original draft, Writing – review & editing. **Lisa E. Brandenburg:** Formal analysis, Investigation, Validation, Writing – review & editing. **Cristina Casadidio:** Investigation, Resources, Writing – original draft, Writing – review & editing. **Johanna Walther:** Resources, Writing – review & editing. **Bianca Bonetto Moreno Garcia:** Visualization, Writing – review & editing. **Jan Spanholtz:** Conceptualization, Resources, Writing – review & editing. **Monica Raimo:** Conceptualization, Project administration, Supervision, Writing – review & editing. **Wim E. Hennink:** Resources, Supervision, Writing – review & editing. **Enrico Mastrobattista:** Conceptualization, Methodology, Resources, Supervision, Writing – review & editing. **Massimiliano Caiazzo:** Writing – review & editing, Conceptualization, Funding acquisition, Methodology, Project administration, Resources, Supervision.

Declaration of Competing Interest

The authors declare no conflict of interest.

Data availability

No data was used for the research described in the article.

Acknowledgments

The authors thank Vivian Hegeman for her help with the statistical analysis, Bo Lou and Erik R. Hebels for the helpful discussions on polymeric synthesis, Danny Wilbie for his help with flow cytometry and Flowlogic software, Ewa Kasprzak for her help in setting up the electroporation parameters, Olivier de Jong for providing us with the PEI polymer, Glycostem Therapeutics B.V. for donating us the cord blood-derived NK cells, and last but not least Raymond Schiffelers' group at UMC Utrecht and NanoCell Therapeutics for the access to the NanoAssemblr microfluidics equipment.

Appendix A. Supplementary data

Supplementary data to this article can be found online at https://doi.org/10.1016/j.jconrel.2023.08.014.

References

[1] J.E. Cohen, S. Merims, S. Frank, R. Engelstein, T. Peretz, M. Lotem, Adoptive cell therapy: past, present and future, Immunotherapy. 9 (2017) 183–196, https://doi.org/10.2217/imt-2016-0112.
[2] D.B. Johnson, C.A. Nebhan, J.J. Moslehi, J.M. Balko, Immune-checkpoint inhibitors: long-term implications of toxicity, Nat. Rev. Clin. Oncol. 19 (2022) 254–267, https://doi.org/10.1038/s41571-022-00600-w.
[3] J.D. Chan, J. Lai, C.Y. Slaney, A. Kallies, P.A. Beavis, P.K. Darcy, Cellular networks controlling T cell persistence in adoptive cell therapy, Nat. Rev. Immunol. 21 (2021) 769–784, https://doi.org/10.1038/s41577-021-00539-6.
[4] B. Wolf, S. Zimmermann, C. Arber, M. Irving, L. Trueb, G. Coukos, Safety and tolerability of adoptive cell therapy in Cancer, Drug Saf. 42 (2019) 315–334, https://doi.org/10.1007/s40264-018-0779-3.
[5] T. Haslauer, R. Greil, N. Zaborsky, R. Geisberger, Car t-cell therapy in hematological malignancies, Int. J. Mol. Sci. 22 (2021) 8996, https://doi.org/10.3390/ijms22168996.
[6] K. Rezvani, Adoptive cell therapy using engineered natural killer cells, Bone Marrow Transplant. 54 (2019) 785–788, https://doi.org/10.1038/s41409-019-0601-6.
[7] J. Rosenberg, J. Huang, CD8+ T cells and NK cells: parallel and complementary soldiers of immunotherapy, Curr. Opin. Chem. Eng. 19 (2018) 9–20, https://doi.org/10.1016/j.coche.2017.11.006.
[8] N. Kim, H.H. Lee, H.J. Lee, W.S. Choi, J. Lee, H.S. Kim, Natural killer cells as a promising therapeutic target for cancer immunotherapy, Arch. Pharm. Res. (2019) 591–606, https://doi.org/10.1007/s12272-019-01143-y.

[9] N.L. Kok, D. Panella, A.M. Georgoudaki, H. Liu, D. Özkazanc, L. Kučerová, A. D. Duru, J. Spanholtz, M. Raimo, Natural killer cells in clinical development as non - engineered, engineered, and combination therapies, J. Hematol. Oncol. 15 (2022) 1–55, https://doi.org/10.1186/s13045-022-01382-5.

[10] H. Ebrahimiyan, A. Tamimi, B. Shokoohian, N. Minaei, A. Memarnejadian, N. Hossein-Khannazer, M. Hassan, M. Vosough, Novel insights in CAR-NK cells beyond CAR-T cell technology; promising advantages, Int. Immunopharmacol. 106 (2022), https://doi.org/10.1016/j.intimp.2022.108587.

[11] J.E. Rubnitz, H. Inaba, R.C. Ribeiro, S. Pounds, B. Rooney, T. Bell, C.H. Pui, W. Leung, NKAML: a pilot study to determine the safety and feasibility of haploidentical natural killer cell transplantation in childhood acute myeloid leukemia, J. Clin. Oncol. 28 (2010) 955–959, https://doi.org/10.1200/JCO.2009.24.4590.

[12] J. Xia, S. Minamino, K. Kuwabara, CAR-expressing NK cells for cancer therapy: a new hope, Biosci. Trends. 14 (2020) 354–359, https://doi.org/10.5582/bst.2020.03308.

[13] E. Vivier, E. Tomasello, M. Baratin, T. Walzer, S. Ugolini, Functions of natural killer cells, Nat. Immunol. 9 (2008) 503–510, https://doi.org/10.1038/ni1582.

[14] I. Prager, C. Watzl, Mechanisms of natural killer cell-mediated cellular cytotoxicity, J. Leukoc. Biol. 105 (2019) 1319–1329, https://doi.org/10.1002/JLB.MR0718-269R.

[15] J.A. Myers, J.S. Miller, Exploring the NK cell platform for cancer immunotherapy, Nat. Rev. Clin. Oncol. 18 (2021) 85–100, https://doi.org/10.1038/s41571-020-0426-7.

[16] T. Michel, M. Ollert, J. Zimmer, A hot topic: Cancer immunotherapy and natural killer cells, Int. J. Mol. Sci. 23 (2022) 797, https://doi.org/10.3390/ijms23020797.

[17] P. Parham, P.J. Norman, L. Abi-Rached, L.A. Guethlein, Human-specific evolution of killer cell immunoglobulin-like receptor recognition of major histocompatibility complex class I molecules, Philos. Trans. R. Soc. B Biol. Sci. 367 (2012) 800–811, https://doi.org/10.1098/rstb.2011.0266.

[18] E.O. Long, Negative signaling by inhibitory receptors: the NK cell paradigm, Immunol. Rev. 224 (2008) 70–84, https://doi.org/10.1111/j.1600-065X.2008.00660.x.

[19] L.L. Lanier, Up on the tightrope: natural killer cell activation and inhibition, Nat. Immunol. 9 (2008) 495–502, https://doi.org/10.1038/ni1581.

[20] T. Ingegnere, F.R. Mariotti, A. Pelosi, C. Quintarelli, B. De Angelis, N. Tumino, F. Besi, C. Cantoni, F. Locatelli, P. Vacca, L. Moretta, Human CAR NK cells: a new non-viral method allowing high efficient transfection and strong tumor cell killing, Front. Immunol. 10 (2019), https://doi.org/10.3389/fimmu.2019.00957.

[21] I. Prager, C. Liesche, H. Van Ooijen, D. Urlaub, Q. Verron, N. Sandström, F. Fasbender, M. Claus, R. Eils, J. Beaudouin, B. Önfelt, C. Watzl, NK cells switch from granzyme B to death receptor-mediated cytotoxicity during serial killing, J. Exp. Med. 216 (2019) 2113–2127, https://doi.org/10.1084/jem.20181454.

[22] J. Domagala, M. Lachota, M. Klopotowska, A. Graczyk-Jarzynka, A. Domagala, A. Zhylko, K. Soroczynska, M. Winiarska, The tumor microenvironment—a metabolic obstacle to NK cells' activity, Cancers (Basel). 12 (2020) 3542, https://doi.org/10.3390/cancers12123542.

[23] P.R. Kennedy, M. Felices, J.S. Miller, Challenges to the broad application of allogeneic natural killer cell immunotherapy of cancer, Stem Cell Res Ther 13 (2022), https://doi.org/10.1186/s13287-022-02769-4.

[24] M. Carlsten, E. Levy, A. Karambelkar, L. Li, R. Reger, M. Berg, M.V. Peshwa, R. W. Childs, Efficient mRNA-based genetic engineering of human NK cells with high-affinity CD16 and CCR7 augments rituximab-induced ADCC against lymphoma and targets NK cell migration toward the lymph node-associated chemokine CCL19, Front. Immunol. 7 (2016), https://doi.org/10.3389/fimmu.2016.00105.

[25] P.S. Kowalski, A. Rudra, L. Miao, D.G. Anderson, Delivering the messenger: advances in technologies for therapeutic mRNA delivery, Mol. Ther. 27 (2019) 710–728, https://doi.org/10.1016/j.ymthe.2019.02.012.

[26] J.A. Kulkarni, D. Witzigmann, S.B. Thomson, S. Chen, B.R. Leavitt, P.R. Cullis, R. van der Meel, The current landscape of nucleic acid therapeutics, Nat. Nanotechnol. 16 (2021) 630–643, https://doi.org/10.1038/s41565-021-00898-0.

[27] L. Xiao, D. Cen, H. Gan, Y. Sun, N. Huang, H. Xiong, Q. Jin, L. Su, X. Liu, K. Wang, G. Yan, T. Dong, S. Wu, P. Zhou, J. Zhang, W. Liang, J. Ren, Y. Teng, C. Chen, X. H. Xu, Adoptive transfer of NKG2D CAR mRNA-engineered natural killer cells in colorectal Cancer patients, Mol. Ther. 27 (2019) 1114–1125, https://doi.org/10.1016/j.ymthe.2019.03.011.

[28] A.J. Wilk, N.L.B. Weidenbacher, R. Vergara, O.A.W. Haabeth, R. Levy, R. M. Waymouth, P.A. Wender, C.A. Blish, Charge-altering releasable transporters enable phenotypic manipulation of natural killer cells for cancer immunotherapy, Blood Adv. 4 (2020) 4244–4255, https://doi.org/10.1182/BLOODADVANCES.2020002355.

[29] M.J. Mitchell, M.M. Billingsley, R.M. Haley, M.E. Wechsler, N.A. Peppas, R. Langer, Engineering precision nanoparticles for drug delivery, Nat. Rev. Drug Discov. 20 (2021) 101–124, https://doi.org/10.1038/s41573-020-0090-8.

[30] J.A. Kulkarni, P.R. Cullis, R. Van Der Meel, Lipid nanoparticles enabling gene therapies: from concepts to clinical utility, Nucleic Acid Ther. 28 (2018) 146–157, https://doi.org/10.1089/nat.2018.0721.

[31] B. Lou, S. De Koker, C.Y.J. Lau, W.E. Hennink, E. Mastrobattista, MRNA Polyplexes with post-conjugated GALA peptides efficiently target, transfect, and activate antigen presenting cells, Bioconjug. Chem. 30 (2018) 461–475, https://doi.org/10.1021/acs.bioconjchem.8b00524.

[32] P. Van De Wetering, N.M.E. Schuurmans-Nieuwenbroek, W.E. Hennink, G. Storm, Comparative transfection studies of human ovarian carcinoma cells in vitro, ex vivo and in vivo with poly(2-(dimethylamino)ethyl methacrylate)-based Polyplexes, J. Gene Med. 1 (1999) 156–165, https://doi.org/10.1002/(SICI)1521-2254(199905/06)1:3<156::AID-JGM29>3.0.CO;2-O.

[33] S. Sabnis, E.S. Kumarasinghe, T. Salerno, C. Mihai, T. Ketova, J.J. Senn, A. Lynn, A. Bulychev, I. McFadyen, J. Chan, Ö. Almarsson, M.G. Stanton, K.E. Benenato, A novel amino lipid series for mRNA delivery: improved endosomal escape and sustained pharmacology and safety in non-human Primates, Mol. Ther. 26 (2018) 1509–1519, https://doi.org/10.1016/j.ymthe.2018.03.010.

[34] L. Novo, E.V.B. Van Gaal, E. Mastrobattista, C.F. Van Nostrum, W.E. Hennink, Decationized crosslinked polyplexes for redox-triggered gene delivery, J. Control. Release 169 (2013) 246–256, https://doi.org/10.1016/j.jconrel.2013.03.035.

[35] J. Luten, N. Akeroyd, A. Funhoff, M.C. Lok, H. Talsma, W.E. Hennink, Methacrylamide polymers with hydrolysis-sensitive cationic side groups as degradable gene carriers, Bioconjug. Chem. 17 (2006) 1077–1084, https://doi.org/10.1021/bc060068p.

[36] G.T. Zugates, D.G. Anderson, S.R. Little, I.E.B. Lawhorn, R. Langer, Synthesis of poly(β-amino ester)s with thiol-reactive side chains for DNA delivery, J. Am. Chem. Soc. 128 (2006) 12726–12734, https://doi.org/10.1021/ja061570n.

[37] M.F. Ebbesen, D.H. Schaffert, M.L. Crowley, D. Oupický, K.A. Howard, Synthesis of click-reactive HPMA copolymers using RAFT polymerization for drug delivery applications, J. Polym. Sci. Part A Polym. Chem. 51 (2013) 5091–5099, https://doi.org/10.1002/pola.26941.

[38] S. Alishetty, M. Carrasco, M.-G. Alameh, M. Paige, H. Said, L. Wright, A. Narayanan, F. Alem, K. Hernandez, P. Gillevet, O. Soliman, P. Hicks, T. Manzoni, P. Bates, A. Stephens-Shields, T. Cleveland, A. Grishaev, D. Weissman, M. Buschmann, Novel Lipid Nanoparticle Provides Potent SARS-CoV-2 mRNA Vaccine at Low Dose with Low Local Reactogenicity, High Thermostability and Limited Systemic Biodistribution, 2021.

[39] B. Lou, A. De Beuckelaer, G.R. Dakwar, K. Remaut, J. Grooten, K. Braeckmans, B. G. De Geest, E. Mastrobattista, S. De Koker, W.E. Hennink, Post-PEGylated and crosslinked polymeric ssRNA nanocomplexes as adjuvants targeting lymph nodes with increased cytolytic T cell inducing properties, J. Control. Release 284 (2018) 73–83, https://doi.org/10.1016/j.jconrel.2018.06.010.

[40] M. Bagheri, J. Bresseleers, A. Varela-Moreira, O. Sandre, S.A. Meeuwissen, R. M. Schiffelers, J.M. Metselaar, C.F. Van Nostrum, J.C.M. Van Hest, W.E. Hennink, Effect of formulation and processing parameters on the size of mPEG- b-p(HPMA-Bz) polymeric micelles, Langmuir. 34 (2018) 15495–15506, https://doi.org/10.1021/acs.langmuir.8b03576.

[41] P. Van De Wetering, J.Y. Cherng, H. Talsma, W.E. Hennink, Relation between transfection efficiency and cytotoxicity of poly((2-dimethylamino)ethyl methacrylate)/plasmid complexes, J. Control. Release 49 (1997) 59–69, https://doi.org/10.1016/S0168-3659(97)00059-X.

[42] J. Spanholtz, F. Preijers, M. Tordoir, C. Trilsbeek, J. Paardekooper, T. de Witte, N. Schaap, H. Dolstra, Clinical-grade generation of active NK cells from cord blood hematopoietic progenitor cells for immunotherapy using a closed-system culture process, PLoS One 6 (2011), e20740, https://doi.org/10.1371/journal.pone.0020740.

[43] J. Veluchamy, An off the shelf, GMP compliant,fully closed and semi-automated large-scale production system for allogeneic NK cells, Cytotherapy. 22 (2020) S161–S162, https://doi.org/10.1016/j.jcyt.2020.03.338.

[44] Z. Dai, T. Gjetting, M.A. Mattebjerg, C. Wu, T.L. Andresen, Elucidating the interplay between DNA-condensing and free polycations in gene transfection through a mechanistic study of linear and branched PEI, Biomaterials. 32 (2011) 8626–8634, https://doi.org/10.1016/j.biomaterials.2011.07.044.

[45] S. Boeckle, K. von Gersdorff, S. van der Piepen, C. Culmsee, E. Wagner, M. Ogris, Purification of polyethylenimine polyplexes highlights the role of free polycations in gene transfer, J. Gene Med. 6 (2004) 1102–1111, https://doi.org/10.1002/jgm.598.

[46] J. Cheng, X. Tang, J. Zhao, T. Shi, P. Zhao, C. Lin, Multifunctional cationic polyurethanes designed for non-viral cancer gene therapy, Acta Biomater. 30 (2016) 155–167, https://doi.org/10.1016/j.actbio.2015.11.048.

[47] S. Vaidyanathan, J. Chen, B.G. Orr, M.M. Banaszak Holl, Cationic polymer intercalation into the lipid membrane enables intact Polyplex DNA escape from endosomes for gene delivery, Mol. Pharm. 13 (2016) 1967–1978, https://doi.org/10.1021/acs.molpharmaceut.6b00139.

[48] S.H. Huh, H.J. Do, H.Y. Lim, D.K. Kim, S.J. Choi, H. Song, N.H. Kim, J.K. Park, W. K. Chang, H.M. Chung, J.H. Kim, Optimization of 25 kDa linear polyethylenimine for efficient gene delivery, Biologicals. 35 (2007) 165–171, https://doi.org/10.1016/j.biologicals.2006.08.004.

[49] D. Pei, M. Buyanova, Overcoming endosomal entrapment in drug delivery, Bioconjug. Chem. 30 (2019) 273–283, https://doi.org/10.1021/acs.bioconjchem.8b00778.

[50] J.T. Granados-Riveron, G. Aquino-Jarquin, Engineering of the current nucleoside-modified mRNA-LNP vaccines against SARS-CoV-2, Biomed. Pharmacother. 142 (2021), 111953, https://doi.org/10.1016/j.biopha.2021.111953.

[51] S. Patel, N. Ashwanikumar, E. Robinson, Y. Xia, C. Mihai, J.P. Griffith, S. Hou, A. A. Esposito, T. Ketova, K. Welsher, J.L. Joyal, Ö. Almarsson, G. Sahay, Naturally-occurring cholesterol analogues in lipid nanoparticles induce polymorphic shape and enhance intracellular delivery of mRNA, Nat. Commun. 11 (2020), https://doi.org/10.1038/s41467-020-14527-2.

[52] M. Herrera, J. Kim, Y. Eygeris, A. Jozic, G. Sahay, Illuminating endosomal escape of polymorphic lipid nanoparticles that boost mRNA delivery, Biomater. Sci. 9 (2021) 4289–4300, https://doi.org/10.1039/d0bm01947j.

[53] Y. Eygeris, S. Patel, A. Jozic, G. Sahay, G. Sahay, Deconvoluting lipid nanoparticle structure for messenger RNA delivery, Nano Lett. 20 (2020) 4543–4549, https://doi.org/10.1021/acs.nanolett.0c01386.

[54] E. Kastner, R. Kaur, D. Lowry, B. Moghaddam, A. Wilkinson, Y. Perrie, High-throughput manufacturing of size-tuned liposomes by a new microfluidics method using enhanced statistical tools for characterization, Int. J. Pharm. 477 (2014) 361–368, https://doi.org/10.1016/j.ijpharm.2014.10.030.

[55] M.J.W. Evers, J.A. Kulkarni, R. van der Meel, P.R. Cullis, P. Vader, R.M. Schiffelers, State-of-the-art Design and rapid-mixing production techniques of lipid nanoparticles for nucleic acid delivery, Small Methods. 2 (2018), https://doi.org/10.1002/SMTD.201700375.

[56] T. Batista Napotnik, T. Polajžer, D. Miklavčič, Cell death due to electroporation – a review, Bioelectrochemistry. 141 (2021), 107871, https://doi.org/10.1016/j.bioelechem.2021.107871.

[57] S.A.A. Kooijmans, S. Stremersch, K. Braeckmans, S.C. De Smedt, A. Hendrix, M.J. A. Wood, R.M. Schiffelers, K. Raemdonck, P. Vader, Electroporation-induced siRNA precipitation obscures the efficiency of siRNA loading into extracellular vesicles, J. Control. Release 172 (2013) 229–238, https://doi.org/10.1016/j.jconrel.2013.08.014.

[58] T. Nakamura, T. Nakade, Y. Sato, H. Harashima, Delivering mRNA to a human NK cell line, NK-92 cells, by lipid nanoparticles, Int. J. Pharm. 636 (2023), https://doi.org/10.1016/j.ijpharm.2023.122810.